

Computing Modes of Instability of Parameterized Nonlinear Systems for Vulnerability Assessment

Jinghan Wang and Michael W. Fisher

Abstract—Engineered systems naturally experience large disturbances which have the potential to disrupt desired operation because the system may fail to recover to a desired stable equilibrium point. It is valuable to determine the mechanism of instability when the system is subject to a particular finite-time disturbance, because this information can be used to improve vulnerability detection, and to design controllers to reduce vulnerability. For a large class of nonlinear systems there exists a particular unstable equilibrium point on the region of attraction boundary of the desired stable equilibrium point such that the unstable eigenvector of the Jacobian at this unstable equilibrium point represents the mode of instability for the disturbance. Unfortunately, it is challenging to find this mode of instability, especially in high dimensional systems, because it is often computationally intractable to obtain this particular unstable equilibrium point for a given disturbance. This paper develops a novel algorithm for numerically computing the mode of instability for parameter-dependent nonlinear systems without prior knowledge of the particular unstable equilibrium point, resulting in a computationally efficient method. The key idea is to first consider the setting where the system recovers, and to average the Jacobian along the system trajectory from the post-disturbance state up until the Jacobian becomes stable. As the system approaches inability to recover, the averaged Jacobians converge to the Jacobian at the particular unstable equilibrium point, and can be used to extract the unstable eigenvector representing the mode of instability. Convergence guarantees are provided for computing the mode of instability, both for the theoretical setting in continuous time, and for the proposed algorithm which relies on numerical integration. Numerical examples illustrate the successful application of the method to identify the mechanism of instability in power systems subject to temporary short circuits.

I. INTRODUCTION

Disturbances naturally occur in engineered systems, and may disrupt desired system behavior. For example, temporary short circuits in a power system can lead to blackout conditions. When the system is unable to recover from a given finite-time disturbance to a stable equilibrium point (SEP) representing desired behavior, often there is a particular subset of system states whose coupled dynamics is responsible for this failure to recover. We refer to these lower order dynamics that result in failure to recover as the mechanism of instability of the disturbance [1]. In networked or complex systems, the mechanism of instability typically also reveals the components of the system most responsible for this inability to recover. Determining the mechanism of instability is valuable because focusing on the most important subset of system dynamics for a given disturbance facilitates detecting proximity to vulnerability to the disturbance and designing controllers to reduce this vulnerability [2], [3].

Fix a particular finite-time disturbance, such as a particular short circuit at a particular location in the system, and denote the system state immediately after the disturbance as the post-disturbance initial condition, or initial condition (IC) for short. Whether or not the system recovers from the disturbance to the desired SEP depends on whether the IC lies within the region of attraction of that SEP. When the system is just marginally unable to recover, its IC lies on the region of attraction boundary of the SEP and, for a large class of nonlinear systems, within the stable manifold of some unstable equilibrium point, which is known as the controlling unstable equilibrium point (CUEP) [4]. Generically, the Jacobian at the CUEP has a unique unstable eigenvalue [2] and, as in [3], we define the nonlinear mode of instability to be the corresponding eigenvector of that unstable eigenvalue. In the situations where the system fails to recover, this mode of instability is responsible for driving the system state away from the region of attraction after the disturbance [3], and thus represents the mechanism of instability.

There is a long history on identifying the nonlinear mode of instability. In [5] the mode of instability is computed and then used to identify the coupled oscillators in the system that are the first to lose synchronization in response to a disturbance. More recent work includes using the mode of instability to quantify the relative contributions of each state to transient dynamics using CUEP-based participation factor analysis with its corresponding unstable eigenvector [6]. The main method in the literature for computing the mode of instability is to first determine the CUEP, and then directly find the unstable eigenvector of its Jacobian [3]. However, determining the CUEP is itself a challenging problem and can often be intractable in practice [7]. Although several methods exist in the literature for finding the CUEP, including the mode of disturbance method [8], the exit point method (also known as the BCU method) [9], and the shadowing method [10], these methods typically lack rigorous convergence guarantees, may converge to an incorrect equilibrium point or fail to converge at all, and often require many time-consuming simulations, which can lead to prohibitively large computational cost, especially for high dimensional systems.

The main goal of this paper is to develop a computationally efficient method with rigorous convergence guarantees for computing the nonlinear mode of instability without requiring knowledge of the CUEP. This provides guarantees of reliability for correctly computing the mode of instability while avoiding the challenge of identifying the CUEP. While much of the historical work focused on finding the mode of instability for a single vector field, this paper considers the more general and

more challenging case of finding this mode for a parameter-dependent vector field with parameter-dependent IC. This more general setting is adopted here because disturbance recovery often depends on system parameters, which may be uncertain and time-varying. As in [11], we define the recovery boundary to be the boundary in parameter space between the parameter values for which the system recovers from the disturbance and the parameter values for which it fails to recover. In the special case where the parameter is chosen to be the IC, the recovery boundary becomes equal to the region of attraction boundary, so it can be interpreted as a generalization of the region of attraction boundary to assess vulnerability in parameter space.

The method presented in this paper exploits the properties that as parameter values approach the recovery boundary in parameter space, the IC approaches the region of attraction boundary in state space and the amount of time the system trajectory spends near the CUEP diverges towards infinity [12]. For a parameter value for which the system recovers from the disturbance, the key idea of the proposed approach is to average the Jacobian along the system trajectory from the IC until the final time at which the Jacobian transitions from unstable to stable. The intuition is that as parameter values approach the recovery boundary, since the system trajectory spends increasing time near the CUEP, the Jacobians along the system trajectory will spend increasing time close to the Jacobian at the CUEP, and their average will approach the Jacobian at the CUEP. However, it is important to only average along the trajectory until the final time at which the Jacobian transitions to becoming stable, since the remaining portion of the trajectory converges to the SEP and, thus, averaging over the entire trajectory would result in the average approaching the Jacobian at the SEP rather than the Jacobian at the CUEP.

The method presented in this paper relies on prior work [13], [14] to find parameter values on the recovery boundary, and numerically computes this average of the Jacobians as parameter values approach the recovery boundary. We prove that as the parameter values approach the recovery boundary, this average of the Jacobians converges to the true Jacobian at the CUEP. Furthermore, under the same conditions we prove that the average of the Jacobians will have a unique unstable eigenvalue whose corresponding eigenvector converges to the mode of instability. The average of the Jacobians is evaluated in practice using numerical integration of the underlying system trajectory, which introduces approximation errors. Therefore, for the proposed algorithm which relies on numerical integration, we further prove that the approximation of the average of the Jacobians obtained from numerical integration, and its eigenvector corresponding to its unstable eigenvalue, will converge to the true Jacobian at the CUEP and the mode of instability, respectively, in the limit as the time step of the numerical integration approaches zero. Ultimately, the proposed approach is computationally efficient, does not require knowledge of the CUEP, and these convergence guarantees ensure it will reliably compute the mode of instability accurately.

The method is first validated on the simple example of a nonlinear pendulum subject to a disturbance. In this case,

since the system is low dimensional the CUEP and mode of instability can be easily obtained analytically. It is shown that the proposed method accurately computes the mode of instability. Then, the method is applied to determine the mode of instability of a power system containing multiple generators subject to a temporary short circuit at a particular location in the network without attempting to identify the CUEP. The points on the recovery boundary are considered both in one and higher dimensional parameter spaces. The identified modes of instability provide non-intuitive insights into the mechanism of instability, including a case where the generator most responsible for failure to recover is distant from the location of the disturbance, a situation where one generator plays a minimal role for the inability to recover, and that the PSS controllers, which are often associated with the failure to recover, do not exhibit much impact in these cases. This unexpected dynamic behavior is challenging to predict or identify without applying the proposed algorithm.

The remainder of the paper is organized as follows. Section II provides background information. Section III discusses the main results. Section IV shows illustrative examples. Section V provides the proofs. Finally, Section VI offers concluding remarks.

II. BACKGROUND

Let J be a connected smooth manifold that is a subset of \mathbb{R}^m for some integer $m > 0$ representing the parameter space, where \mathbb{R}^m is the m -dimensional Euclidean space. Consider a family of vector fields $f : \mathbb{R}^n \times J \rightarrow \mathbb{R}^n$, parameterized by J , such that f is C^1 and $n > 0$ is an integer. Then for any $p \in J$, we have that $f_p := f(\cdot, p)$ is a vector field on \mathbb{R}^n . We use \dot{x} to denote the time derivative of the dynamic states $x \in \mathbb{R}^n$. We model a particular finite-time parameter-dependent disturbance as a parameter-dependent post-disturbance initial condition, which we simply refer to as the IC $x_0 : J \rightarrow \mathbb{R}^n$ given by $x(0) := x_0(p)$. Hence, we consider the family of ordinary differential equations (ODEs) given for $p \in J$ by

$$\dot{x} = f(x, p), \quad (1)$$

$$x(0) = x_0(p). \quad (2)$$

Let $\phi(x, p, t)$ denote the flow of the vector field f from the IC $x \in \mathbb{R}^n$ at time $t \in \mathbb{R}$ for parameter value $p \in J$. For any subset $T \subset \mathbb{R}$, let $\phi(x, p, T) = \bigcup_{t \in T} \phi(x, p, t)$. For any subsets $J' \subset J$ and $T \subset \mathbb{R}$, let $\phi(x_0(J'), J', T)$ denote the disjoint union $\bigsqcup_{p \in J'} \phi(x_0(p), p, T) = \bigcup_{p \in J'} \phi(x_0(p), p, T) \times \{p\} \subset \mathbb{R}^n \times J$.

Consider a fixed $\tilde{p} \in J$. For any $x \in \mathbb{R}^n$ we say that x is nonwandering under $f_{\tilde{p}}$ if for every open neighborhood U of x and any $T \in \mathbb{R}$, there exists $t \in \mathbb{R}$ of the same sign as T with $|t| > T$ such that $\phi(U, \tilde{p}, t) \cap U \neq \emptyset$. Let $\Omega(f_{\tilde{p}})$ denote the set of all nonwandering points of $f_{\tilde{p}}$, and note that this includes all equilibria and periodic orbits of $f_{\tilde{p}}$, as well as chaotic dynamics and other forms of recurrent behavior. Let a *critical element* $x(\tilde{p})$ be either an equilibrium point or a periodic orbit of $f_{\tilde{p}}$. An equilibrium point $x(\tilde{p})$ of $f_{\tilde{p}}$ is hyperbolic if its linearization $\frac{\partial f}{\partial x}(x(\tilde{p}))$ has no purely imaginary eigenvalues. A periodic orbit $x(\tilde{p})$ of $f_{\tilde{p}}$

is hyperbolic if there exists $x \in x(\tilde{p})$ and a cross section S containing x such that the Poincaré first return map $\tau : S \rightarrow S$ is well-defined and its linearization $\frac{d\tau(x)}{dx}$ has no eigenvalues of norm one. Every hyperbolic critical element $x(\tilde{p})$ of $f_{\tilde{p}}$ possesses a stable manifold $W^s(x(\tilde{p}))$ and an unstable manifold $W^u(x(\tilde{p}))$ where $W^s(x(\tilde{p}))$ ($W^u(x(\tilde{p}))$) consists of all initial conditions that converge to $x(\tilde{p})$ in forwards (backwards) time, respectively. Furthermore, there exist local stable and unstable manifolds, denoted by $W_{\text{loc}}^s(x(\tilde{p}))$ and $W_{\text{loc}}^u(x(\tilde{p}))$, which are invariant in forwards and backwards time, respectively. Furthermore, for any hyperbolic critical element $x(\tilde{p})$ of $f_{\tilde{p}}$, for J sufficiently small and any $p \in J$, there exists a unique hyperbolic critical element $x(p)$ that is equal to $x(\tilde{p})$ at $p = \tilde{p}$, and such that $x(p)$, $W_{\text{loc}}^s(x(p))$, and $W_{\text{loc}}^u(x(p))$ all vary C^1 with p . For any $J' \subset J$, define $x(J') = \sqcup_{p \in J'} x(p) = \cup_{p \in J'} x(p) \times \{p\} \subset \mathbb{R}^n \times J$. Define $W^s(x(J'))$ and $W^u(x(J'))$ analogously.

The notion of a generic C^1 vector field is used to describe typical behavior, similar to the concept of probability one in a probability space. A property that holds for a generic class of C^1 vector fields is therefore considered to represent typical or expected behavior. Since there exists many pathological C^1 vector fields, it is often beneficial to restrict analysis to certain classes of generic C^1 vector fields, which facilitates establishing the theoretical framework for generic vector fields that often would not hold for arbitrary vector fields. For any set A in a topological space, let ∂A denote its topological boundary, \bar{A} its topological closure, and $\text{int } A$ its topological interior. For any point $x \in \mathbb{R}^n$ in state space and any $r > 0$, define $B_r(x)$ to be the open ball of radius r centered at x . For any manifold A and $x \in A$, let $T_x A$ denote the tangent space to A at x . Two manifolds $A, B \subset \mathbb{R}^n$ are transverse if for every $x \in A \cap B$, $T_x A + T_x B = T_x \mathbb{R}^n$. For additional background in differential topology, including the strong and weak C^1 topologies, we refer the reader to [15, Chapter 2]. For more information regarding C^1 distance and ϵ C^1 -close, we refer the reader to the background section in [12].

Suppose $p_0 \in J$ such that f_{p_0} possesses a hyperbolic stable equilibrium point (SEP), denoted by $x^s(p_0)$. Then for J sufficiently small and any $p \in J$, there exists a unique hyperbolic SEP $x^s(p)$ near $x^s(p_0)$. For $p \in J$, we define the region of attraction of $x^s(p)$ to be its stable manifold $W^s(x^s(p))$, and $\partial W^s(x^s(p))$ denotes the region of attraction boundary. For a parameter value $p \in J$, the system recovers from the disturbance if and only if $x_0(p) \in W^s(x^s(p))$. Let the *recovery region* R be the set of parameter values in J for which the system recovers, and define the *recovery boundary* to be its topological boundary ∂R in J . We define parameter values that lie on the recovery boundary as *boundary parameter values*.

Propositions 1 and 2 will be useful for establishing rigorous guarantees for our method to compute the nonlinear mode of instability for a large class of parameterized nonlinear systems. Proposition 1 was proved in [12] and [11], and states that under general assumptions satisfied by a large class of dynamical systems, and for sufficiently small J , the region of attraction boundary in state space varies continuously with respect to parameter, and equals the union of the stable manifolds of the critical elements it contains. Since each parameter value

on the recovery boundary has corresponding IC lying on the region of attraction boundary in state space, and therefore in the stable manifold of some critical element, which we call the *controlling critical element*, and whose unstable manifold intersects the region of attraction. This proposition establishes a direct connection between the recovery boundary in parameter space and the region of attraction boundary in state space, which will be used for proving the theoretical guarantees of the proposed algorithm for computing the mode of instability for parameterized nonlinear systems.

Proposition 1. [11, Theorem 4.17, Corollary 4.18, Theorem 4.21, Corollary 4.23] Assume there exists $p_0 \in J$ such that:

- (i) Every critical element in $\partial W^s(x^s(p_0))$ is hyperbolic.
- (ii) The intersections of the stable and unstable manifolds of the critical elements in $\partial W^s(x^s(p_0))$ are transverse.
- (iii) The intersection of $\partial W^s(x^s(p_0))$ with $\Omega(f_{p_0})$ consists of a finite union of critical elements $\{x^i(p_0)\}_{i \in I}$ where the set I indexes the critical elements that lie on $\partial W^s(x^s(p_0))$.
- (iv) There exists a neighborhood of infinity which contains no nonwandering points of f_{p_0} and no orbits which diverge to infinity in both forwards and backwards time.
- (v) The vector field family $\{f_p\}_{p \in J}$ is strong C^1 continuous and x_0 is C^1 .
- (vi) Certain lower semicontinuous functions over J are continuous at p_0 , see [11, Theorem 4.17] for more details.

Then for J sufficiently small, $\partial W^s(x^s(p))$ varies continuously with p and $\partial W^s(x^s(J)) = \bigcup_{i \in I} W^s(x^i(J))$. For any $p^* \in \partial R$, $x_0(p^*) \in \partial W^s(x^s(p^*))$. Then $x_0(p^*) \in W^s(x^j(p^*))$ for a unique $j \in I$, $x^j(p^*)$ is called the *controlling critical element* for p^* , and $W^s(x^s(p^*)) \cap W^u(x^j(p^*)) \neq \emptyset$.

Remark 1. Note that Assumptions (i), (ii), and (vi) are generic, and it is generically true that $\Omega(f_{p_0})$ is equal to the closure of the union of the critical elements of f_{p_0} [16] (compare to Assumption (iii)), so (iii) is equivalent to a finite number of critical elements, along with this generic condition. Thus, the conditions of Proposition 1 are very general and hold for a large class of realistic engineering system models.

Assumption 1. By Proposition 1, $\partial W^s(x^s(J)) = \bigcup_{i \in I} W^s(x^i(J))$. Assume that $x_0(J)$ is transverse to $W^s(x^i(J))$ for all $i \in I$ [14, Assumption 1].

Remark 2. Assumption 1 is generic because C^1 submanifolds are generically transverse [17, Theorem A.3.20].

Proposition 2. Assume the conditions of Proposition 1 and Assumption 1. Then there exists an open neighborhood N of ∂R such that for generic $p_0 \in N$, there exists a unique boundary parameter value $p^* \in \partial R$ that is closest to p_0 , and that p^* varies C^1 continuously with initial parameter value p_0 [14, Theorem 4].

Remark 3. Proposition 2 shows that for generic initial parameter value p_0 sufficiently close to the recovery boundary, p_0 has a unique closest point on the recovery boundary that varies smoothly with respect to p_0 .

Recent algorithms have been developed for efficiently computing the closest boundary parameter value $p^* \in \partial R$ to an initial value $p_0 \in R$ in high dimensional parameter and state space [14]. Throughout this paper, for $p^* \in \partial R$, let $\lim_{p \rightarrow p^*}$ denote the limit as p approaches p^* from within R , i.e., $\lim_{p \rightarrow p^*, p \in R}$. We let $\|\cdot\|$ denote the Frobenius norm defined as $\|A\|_F = \sqrt{\sum_{i=1}^n \sum_{j=1}^n |A_{ij}|^2}$.

III. MAIN RESULTS

A. Defining Mode of Instability for Parameterized Systems

We begin by generalizing the definition of the nonlinear mode of instability of a disturbance to parameter-dependent vector fields. Let N be the neighborhood of ∂R from Proposition 2, and fix any initial parameter value $p_0 \in N$ belonging to the generic set described in Proposition 2. Then there exists a unique closest boundary parameter value $p^* \in \partial R$ to p_0 . By Proposition 1, there exists a critical element $x^*(p^*)$ in the region of attraction boundary of $x^s(p^*)$ such that $x_0(p^*)$ lies in the stable manifold of $x^*(p^*)$.

Assumption 2. $W^s(x^*(p^*))$ has codimension one.

Remark 4. Assumption 2 is generic [14, Lemma 3].

Assumption 3. $x^*(p^*)$ is an equilibrium point.

Remark 5. For many practical nonlinear systems including power systems, Assumption 3 is ubiquitous and has been observed through numerical experiments on a wide range of realistic models [10].

Under Assumptions 2-3, $x^*(p^*)$ is known as the CUEP, and we denote it by $x^u(p^*)$. Define $A(p^*)$ to be the Jacobian at $x^u(p^*)$:

$$A(p^*) := \frac{\partial f}{\partial x}(x^u(p^*)). \quad (3)$$

By Assumption 2 and Proposition 1(i), $A(p^*)$ has a unique unstable eigenvalue which we denote by $\lambda(p^*)$. The *mode of instability* is defined to be the eigenvector of $A(p^*)$ associated with the eigenvalue $\lambda(p^*)$, and is denoted $v(p^*)$.

B. Obtaining Mode of Instability via Jacobian Averaging

In order to avoid the complexity of determining the CUEP directly, we propose a method that can indirectly calculate the mode of instability without requiring prior knowledge of the CUEP. At the closest boundary parameter value p^* to p_0 , the IC lies in the stable manifold of the CUEP $x^u(p^*)$, and thus the system trajectory converges to $x^u(p^*)$. As p approaches p^* from within the set of recovery values, the system trajectory spends a very large amount of time around the CUEP $x^u(p)$ before converging to $x^s(p)$. Thus, since the Jacobian depends continuously on state and parameter values, it seems natural to approximate $A(p^*)$ (the Jacobian at $x^u(p^*)$) by averaging the Jacobian along the system trajectory for p near p^* .

Unfortunately, averaging the Jacobian along the system trajectory for all time does not approximate $A(p^*)$ well since as time approaches infinity, the system converges to $x^s(p)$. This implies that the Jacobian along the trajectory converges to the Jacobian at $x^s(p)$, and the average over time of

these Jacobians would also converge to the Jacobian at $x^s(p)$ rather than $A(p^*)$. To avoid this, we instead only average the Jacobians along the system trajectory for a finite length of time $t(p)$ given by the supremum of the times at which these Jacobians are unstable. More precisely, we define

$$t(p) := \sup_{\substack{t > 0 \\ \frac{\partial f}{\partial x}(\phi(x_0(p), p, t)) \text{ is unstable}}} t, \quad (4)$$

where $\frac{\partial f}{\partial x}(\phi(x_0(p), p, t))$ is the Jacobian along the system trajectory at time t for parameter value p .

Note that for any p within the set of recovery values, $t(p)$ is finite since the system trajectory converges to $x^s(p)$, and the Jacobian is stable in a neighborhood of $x^s(p)$. The introduction of this $t(p)$ ensures that the values of the Jacobian near the CUEP dominate the average of the Jacobians along the system trajectory, and that this average will converge to $A(p^*)$ as p approaches p^* . To make this precise, define the piecewise function $F : R \cup \partial R \rightarrow \mathbb{R}^{n \times n}$ such that for any $p \in R$, F averages the Jacobians along the system trajectory from the IC up until $t(p)$, i.e.,

$$F(p) := \frac{1}{t(p)} \int_0^{t(p)} \frac{\partial f}{\partial x}(\phi(x_0(p), p, t)) dt. \quad (5)$$

For any $p^* \in \partial R$, $t(p^*) = \infty$ since $x_0(p^*) \in W^s(x^u(p^*))$. Thus, (5) is not defined at p^* , and so for any $p^* \in \partial R$ we define

$$F(p^*) := A(p^*). \quad (6)$$

Theorem 1 justifies the proposed method for computing $A(p^*)$ indirectly. It shows that $F(p)$ will converge to $F(p^*)$ as p approaches p^* from within R , which implies that the average of the Jacobians along the system trajectory computed in (5) converges to $A(p^*)$.

Theorem 1. Assume that p_0 satisfies the conditions of Proposition 2, and that Assumptions 1-2 hold. Then the piecewise function F defined in (5)-(6) is continuous at p^* :

$$\lim_{p \rightarrow p^*} F(p) = F(p^*) = A(p^*). \quad (7)$$

Theorem 2 shows that as p approaches p^* from within R , $F(p)$ has a unique unstable eigenvalue that converges to the unique unstable eigenvalue of $A(p^*)$, and its corresponding unstable eigenvector converges to the mode of instability.

Theorem 2. Assume the conditions of Theorem 1. Then for p sufficiently close to p^* in R , there exists a unique unstable eigenvalue $\lambda(p)$ of $F(p)$, we denote its corresponding unstable eigenvector as $v(p)$, and

$$\lim_{p \rightarrow p^*} \lambda(p) = \lambda(p^*), \quad (8a)$$

$$\lim_{p \rightarrow p^*} v(p) = v(p^*). \quad (8b)$$

C. Algorithm for Numerically Computing Mode of Instability

The results of Section III-B, and in particular the computation of the average of the Jacobians in (5), requires exact evaluation of an integral along the system trajectory. However, determining the exact system trajectory in continuous time is

in general intractable, and so this section extends the results of Section III-B to the practical setting where the system trajectory is approximated via numerical integration. To do so, we will first require a discrete time analog to Theorems 1-2. Let $h > 0$ represent a constant time step. For any integer n , let $T^n(x_0(p), p, h) := \phi(x_0(p), p, nh)$ be the state obtained from the continuous time system (1)-(2) after n time steps starting from IC $x_0(p)$. Analogously to the definition of $t(p)$ in continuous time, define $j(p)$ in discrete time as

$$j(p) := \sup_{\substack{n \in \mathbb{N}, n > 0 \\ \frac{\partial f}{\partial x}(T^n(x_0(p), p, h)) \text{ is unstable}}} n. \quad (9)$$

Finally, analogously to the definition of $F(p)$ in continuous time, we define its discrete approximation $\hat{F}(p)$ by

$$\hat{F}(p) := \frac{1}{j(p)} \sum_{n=0}^{j(p)} \frac{\partial f}{\partial x}(T^n(x_0(p), p, h)). \quad (10)$$

Theorem 3 shows that as p approaches p^* from within R , $\hat{F}(p)$ converges to $A(p^*)$, and it has a unique unstable eigenvalue that converges to the unique unstable eigenvalue of $A(p^*)$, and its corresponding unstable eigenvector converges to the mode of instability.

Theorem 3. *Assume the conditions of Theorem 1, and fix any time step $h > 0$. Then for p sufficiently close to p^* in R , there exists a unique unstable eigenvalue $\hat{\lambda}(p)$ of $\hat{F}(p)$, let $\hat{v}(p)$ denote its corresponding unstable eigenvector, and*

$$\lim_{p \rightarrow p^*} \hat{F}(p) = A(p^*), \quad (11a)$$

$$\lim_{p \rightarrow p^*} \hat{\lambda}(p) = \lambda(p^*), \quad (11b)$$

$$\lim_{p \rightarrow p^*} \hat{v}(p) = v(p^*). \quad (11c)$$

To derive practical guarantees for our approach, fix any autonomous constant step size numerical integration scheme with the property that for any IC x_0 and any time $t > 0$, the system state obtained from numerical integration after n time steps (where $n = \inf_{nh \geq t} n \in \mathbb{N}$) converges to $\phi(x_0, p, t)$ as the time step h approaches 0. The approximation error resulting from numerical integration can change the recovery boundary and, thereby, change the value of p^* , so let $p^*(h)$ denote the unique closest boundary parameter value on the recovery boundary to p_0 for the chosen integration scheme and the step size h . Define $\hat{j}(p)$ to be the value of $j(p)$ obtained from (9) when T^n is approximated using numerical integration. Similarly, define $\hat{F}(p)$ to be the value of $\hat{F}(p)$ obtained from (10) when T^n is approximated using numerical integration. For h sufficiently small, there exist $x_h^s(p)$ near $x^s(p)$ which is the hyperbolic SEP, and $x_h^u(p)$ near $x^u(p)$ which is the hyperbolic unstable equilibrium point, when T^n is approximated using numerical integration, Theorem 4 shows that as h approaches 0, $p^*(h)$ converges to p^* . As p approaches $p^*(h)$ from within the set of recovery values, $\hat{F}(p)$ converges to the Jacobian at $x_h^u(p^*(h))$. As h approaches zero, $\hat{F}(p^*(h))$ converges to $A(p^*)$, and it has a unique unstable eigenvalue that converges to the unique unstable eigenvalue of $A(p^*)$,

and its corresponding unstable eigenvector converges to the mode of instability.

Theorem 4. *Assume the conditions of Theorem 1. Then for $h > 0$ sufficiently small,*

$$\lim_{h \rightarrow 0} p^*(h) = p^*, \quad (12a)$$

$$\lim_{p \rightarrow p^*(h)} \tilde{F}(p) = \frac{\partial f}{\partial x}(x_h^u(p^*(h))), \quad (12b)$$

$$\lim_{h \rightarrow 0} \lim_{p \rightarrow p^*(h)} \tilde{F}(p) = A(p^*), \quad (12c)$$

and there exists a unique unstable eigenvalue $\tilde{\lambda}(p)$ of $\tilde{F}(p)$, with corresponding unstable eigenvector $\tilde{v}(p)$, and

$$\lim_{h \rightarrow 0} \lim_{p \rightarrow p^*(h)} \tilde{\lambda}(p) = \lambda(p^*), \quad (13a)$$

$$\lim_{h \rightarrow 0} \lim_{p \rightarrow p^*(h)} \tilde{v}(p) = v(p^*). \quad (13b)$$

IV. NUMERICAL EXAMPLES

A. Damped, Driven Nonlinear Pendulum Example

To illustrate the algorithm of Section III-C and the results of Theorem 4, we first consider the simple example of a damped, driven nonlinear pendulum with constant driving force. For this simple example, it is straightforward to compute the mode of instability analytically by directly finding the CUEP, so this example can be used as a benchmark to validate the proposed algorithm. The dynamics are given by

$$\dot{x}_1 = x_2, \quad (14)$$

$$\dot{x}_2 = -c_1 \sin(x_1) - c_2 x_2 + c_3, \quad (15)$$

where $c_1, c_2, c_3 > 0$ are real parameters and $x = (x_1, x_2) \in \mathbb{R}^2$. Physically, x_1 represents the angle of the pendulum, x_2 its angular velocity, c_1 the square of the natural frequency of the pendulum (under the small angle approximation), c_2 a damping coefficient due to air drag, and c_3 the constant driving torque. Using the simple power system model of a single machine infinite bus [18], (14)-(15) can also be interpreted as an electrical generator, with (x_1, x_2) the angle and angular velocity of the turbine, c_1 a constant determining the electrical torque supplied by the generator, c_2 a damping coefficient, and c_3 the constant driving mechanical torque.

For the demonstration below, we set $c = (c_1, c_2, c_3) = (2, 0.5, 1.5)$. This system possesses one SEP at $(0.848, 0)$ and one UEP at $(2.294, 0)$. As we vary the parameter values c_1, c_2 , and/or c_3 , the SEP and UEP will also vary.

We establish an IC to (14)-(15) as the output of the following related system which models a finite-time disturbance:

$$\dot{z}_1 = z_2, \quad (16)$$

$$\dot{z}_2 = -c_2 z_2 + c_3, \quad (17)$$

starting from the SEP and integrating for time $t = 0.8$ seconds, which is the length of time the disturbance is active. This yields the post-disturbance IC for (14)-(15). If (14)-(15) are interpreted as an electrical generator, then (16)-(17) represent a temporary short circuit across the terminals of the generator, which is modeled by setting the electrical torque term in (14)-(15) to zero temporarily, resulting in (16)-(17).

For simplicity, consider the one-dimensional parameter space consisting of just the single parameter $p = c_3$ which we will subsequently treat as a free parameter, with all other parameters constant, and let $p_0 = 1.5$. We set the time step $h = 0.02$ seconds, use trapezoidal integration for the numerical integration, and solve each trapezoidal integration step using the Newton-Raphson method with a tolerance of 10^{-15} . Then the numerical integration of (16)-(17) yields the IC, and the numerical integration of (14)-(15) provides the full system trajectory, which is used to calculate $\tilde{F}(p)$ using (10).

Since the parameter space is one-dimensional in this case, the closest boundary parameter value $p^*(h)$ to p_0 can be found using a backtracking line search performed by bisection. Due to finite numerical precision, and since ∂R is a set of measure zero, in general we cannot numerically compute $p^*(h)$ which lies exactly on ∂R . Instead, we numerically approximate $p^*(h)$ to arbitrary accuracy with a value that lies just inside R . For the remainder of Section IV, we therefore abuse notation and let $p^*(h)$ denote this numerical approximation, which lies slightly inside R , rather than the exact theoretical boundary value. Using the bisection method, we determine that $p^*(0.02) = 1.5686$. In this case, the system with $p = p^*(0.02)$ has two equilibrium points (where the angle is restricted to a single interval of length 2π since the angle is defined modulo 2π), one of which is the SEP where the system begins prior to the disturbance, while the other is a UEP that can be shown to be the CUEP for this disturbance (see Fig. 1), consistent with Assumption 3.

Fig. 2 shows the value of $p^*(h)$ for different values of h : $h \in \{0.02, 0.04, 0.08, 0.1, 0.2, 0.4, 0.8\}$. The graph of $p^*(h)$ versus h becomes a flat line as h gets sufficiently small, which shows that $p^*(h)$ converges to the constant p^* as h approaches zero, consistent with (12a). Let $p^*(0.02)$ be the approximation of the exact theoretical boundary parameter value. For the same values of h , $\left\| \tilde{F}(p^*(h)) - \frac{\partial f}{\partial x}(x_h^u(p^*(h))) \right\| < 6.7\%$, which is consistent with (12b). Fig. 3 shows the value of $\left\| \tilde{F}(p^*(h)) - A(p^*(0.02)) \right\|$ for the same values of h , which shows that $\tilde{F}(p^*(h))$ converges to the true Jacobian as h approaches zero, consistent with (12c). Fig. 4 and Fig. 5 show $\left| \tilde{\lambda}(p^*(h)) - \lambda(p^*(0.02)) \right|$ and $\|\tilde{v}(p^*(h)) - v(p^*(0.02))\|_2$ for the same values of h , which shows that the unstable eigenvalue and its associated eigenvector of $\tilde{F}(p^*(h))$ converge to the unstable eigenvalue of the true Jacobian and the mode of instability, respectively, as h approaches zero, consistent with (13a) and (13b). As the CUEP $x_{0.02}^u(p^*(0.02))$ is known and available analytically, the Jacobian at the CUEP, $A(p^*(0.02))$, can therefore be computed directly and exactly. Consistent with Assumption 2, it has a single unstable eigenvalue, and its corresponding unstable eigenvector is $v(p^*(0.02)) = \begin{bmatrix} 0.7464 \\ 0.6655 \end{bmatrix}$. Let $\hat{p} = p^*(0.02)$ in this case, and note that $\hat{p} \in R$ and is very close to the exact theoretical boundary value. Numerically computing $\tilde{F}(\hat{p})$ from the system trajectory, consistent with Theorem 4, it is shown to have a single unstable eigenvalue with associated unstable eigenvector $\tilde{v}(\hat{p}) = \begin{bmatrix} 0.7569 \\ 0.6536 \end{bmatrix}$. Thus, $\|\tilde{v}(\hat{p}) - v(p^*(0.02))\|_2 < 0.016$, so

$\tilde{v}(\hat{p})$ and $v(p^*(0.02))$ have less than 1.6% difference since both are normalized to unit length. Fig. 1 also shows the region of attraction boundary and the mode of instability at \hat{p} . Therefore, this illustrates that the nonlinear mode of instability of this low dimensional system can be accurately computed by the proposed algorithm.

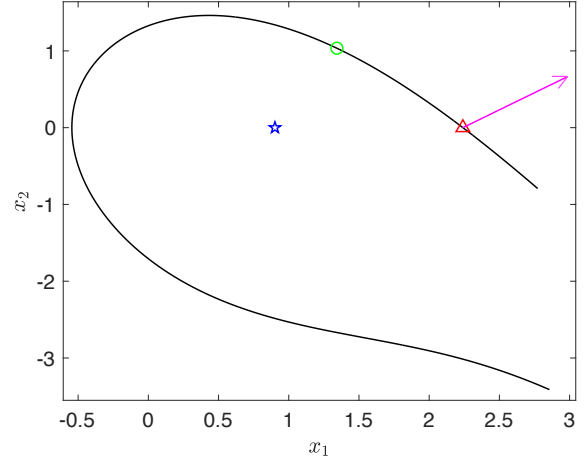


Fig. 1. The region of attraction boundary $\partial W^s(x_{0.02}^s(\hat{p}))$ (solid black line) of the SEP $x_{0.02}^s(\hat{p})$ (blue star) of equations (16)-(17) is shown. It is equal to $W^s(x_{0.02}^u(\hat{p}))$ where $x_{0.02}^u(\hat{p})$ (red triangle) is the UEP that can be shown to be the CUEP for the given disturbance. The IC $x_0(\hat{p})$ (green circle) is shown. The unstable eigenvector $v(\hat{p})$ of $\frac{\partial f}{\partial x}(x_{0.02}^u(\hat{p}))$ (solid magenta line with an arrow), which is the mode of instability for the disturbance, is shown.

B. IEEE 9-Bus Power System

Next, the algorithm described in Section III-C is applied to the more complex example of the IEEE 9-bus power system [19], where the mode of instability is not so straightforward to obtain analytically. As shown in Fig. 6, this is a network consisting of nine nodes that contains three synchronous generators, three loads, six transmission lines, and three transformers. Each generator is modeled using a 4th order synchronous machine model, along with an Active Voltage Regulator (AVR) and Power System Stabilizer (PSS) for control, which are modeled according to the IEEE standard ST1C and PSS1A models [20], respectively. The loads are modeled as constant power loads. The dimension of the dynamic states for this system is 60. The disturbance considered is a temporary short circuit, known as a fault, at the terminals of generator three. The system is initially at a SEP, then the fault occurs at 0.02 seconds. It lasts for 0.2 seconds and is cleared at 0.22 seconds. For this nonlinear power system model with higher dimensions, the mode of instability is determined without direct identification of the CUEP using the algorithm from Section III-C.

Many model parameters of the system are of interest for recovery considerations. The moment of inertia scaling factor multiplies the moment of inertia of all three synchronous generators simultaneously. The gains of the AVR controllers can help to capture the impact of controller turning on system stability and the gains of the PSS controllers are crucial

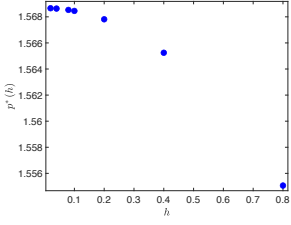


Fig. 2. The closest boundary parameter value $p^*(h)$ to p_0 as a function of h .

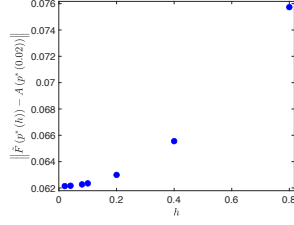


Fig. 3. The norm of the difference between $\tilde{F}(p^*(h))$ and $A(p^*(0.02))$ as a function of h .

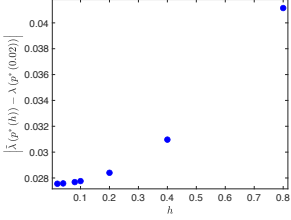


Fig. 4. The absolute value of the difference between the unstable eigenvalues $\tilde{\lambda}(p^*(h))$ of $\tilde{F}(p^*(h))$ and $\lambda(p^*(0.02))$ of $A(p^*(0.02))$ as a function of h .

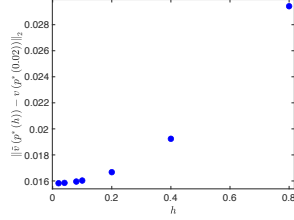


Fig. 5. The norm of the difference between the unstable eigenvectors $\tilde{v}(p^*(h))$ of $\tilde{F}(p^*(h))$ and $v(p^*(0.02))$ of $A(p^*(0.02))$ as a function of h .

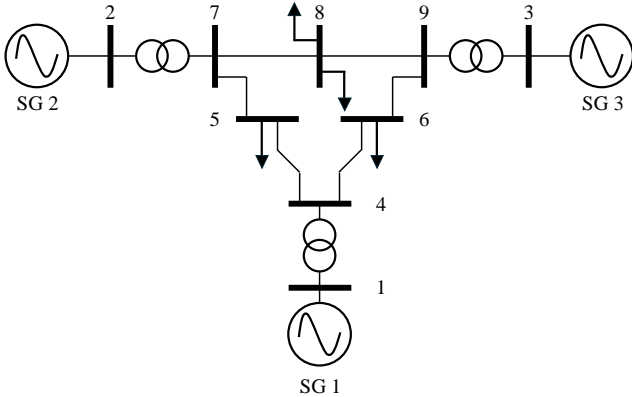


Fig. 6. IEEE 9-Bus Power System (SG = synchronous generator).

for enhancing system stability by improving the damping of low-frequency oscillations in power systems. The active and reactive power loads are modeled using the standard exponential form of a voltage-dependent load model. The voltage exponents are set uniformly for all active power loads and similarly for all reactive power loads. As load is often uncertain, given the complexity of modeling load dynamics, these parameters can help to capture the impact of uncertain load behavior on system recoverability.

To demonstrate the effectiveness of the proposed algorithm, we first consider the one-dimensional parameter space with the parameter of interest being the moment of inertia scaling factor. We use trapezoidal integration with the Newton-Raphson method for the numerical integration with a fixed time step of $h = \frac{1}{60}$ seconds and a tolerance of 10^{-10} . This choice of h represents a single cycle of the 60 Hz AC voltage

and, thus, is faster than all other dynamics explicitly included in the system model, so it represents a choice of h that is close to zero for this application. Using the backtracking line search performed by bisection, or using the method from [14], which finds the closest point on the recovery boundary in one-dimensional parameter space, we compute the boundary value of the moment of inertia scaling factor to be $p^*(\frac{1}{60}) = 0.8724$, which is very close to the exact theoretical boundary value. For this example, we do not know the location of the CUEP, so we are unable to compute $v(p^*(\frac{1}{60}))$ directly from $A(p^*(\frac{1}{60}))$. Instead, we set $\hat{p} = p^*(\frac{1}{60})$, and numerically compute $F(\hat{p})$.

Consistent with Theorem 4, $\tilde{F}(\hat{p})$ has exactly one unstable eigenvalue $\tilde{\lambda}(\hat{p})$. As the choice of h is close to zero for this application, by Theorem 4 its corresponding eigenvector $\tilde{v}(\hat{p})$ is a close approximation to the true mode of instability. Table I shows the components of $\tilde{v}(\hat{p})$ other than those which are close to zero. The components of ω_1 , ω_2 , and ω_3 of $\tilde{v}(\hat{p})$ correspond to the frequency components of generator one, generator two, and generator three, respectively. The components of θ_1 , θ_2 , and θ_3 of $\tilde{v}(\hat{p})$ correspond to the angle of generator one, generator two, and generator three, respectively. The components of x_1 , x_2 , and x_3 correspond to the internal state of the AVR of generator one, generator two, and generator three, respectively.

ω_1	ω_2	ω_3
-0.0112	0.7594	0.4227
θ_1	θ_2	θ_3
-0.0026	0.1754	0.0977
x_1	x_2	x_3
0.0863	0.3473	0.2673

TABLE I
COMPONENTS OF $\tilde{v}(\hat{p})$ REPRESENTING THE FREQUENCIES ω , ANGLES θ , AND THE INTERNAL STATE OF THE AVR x FOR THE THREE SYNCHRONOUS GENERATORS IN THE CASE OF ONE-DIMENSIONAL PARAMETER SPACE.

The mode of instability, as shown in Table I, reveals the subset of dynamics responsible for failure to recover from the fault. In particular, among the three generators, the frequency component, angle component, and the AVR internal state component of generator two are the largest in magnitude. This leads to the non-intuitive information that generator two is most responsible for the failure to recover from the disturbance, even though the disturbance originates at a distant location from generator two (near generator three). To further validate this observation, we plot the frequency dynamics of all three generators before they achieve synchronism, as shown in Fig. 7. The figure shows that the frequency of generator two has larger amplitude oscillations after the disturbance has occurred than the frequencies of the other two generators. Fig. 8 shows the angle of generator three relative to generator one and the angle of generator two relative to generator one as a function of time. We observe that the relative angle of generator two has larger amplitude oscillations after the disturbance has occurred than the relative angle of generator three, indicative of generator two's role as the generator most important to the mechanism of instability for the disturbance. Fig. 9 shows the dynamics for the internal state of the AVR of all three generators. It shows that the internal state of

the AVR of generator two has a larger initial transient than the internal state of the AVR of generator one and generator three, which indicates that generator two is most important for determining whether the system will fail to recover from the disturbance. In addition, Table I shows that the frequency component, angle component, and the AVR internal state component of generator one are very small, indicating that generator one plays a more minimal role in the onset of failure to recover than generators two and three. Furthermore, the components of the internal states of the PSS are close to zero, indicating the nontrivial fact that, unlike for many other faults, for this particular disturbance the PSS controllers do not have a significant contribution to the mechanism of instability.

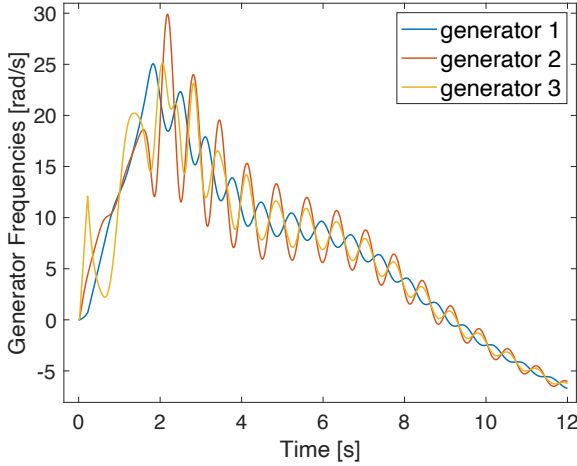


Fig. 7. The frequency dynamics of all three generators before reaching synchronism in the one-dimensional parameter space, where the moment of inertia scaling factor is the parameter of interest, at $p = p^* \left(\frac{1}{60}\right)$.

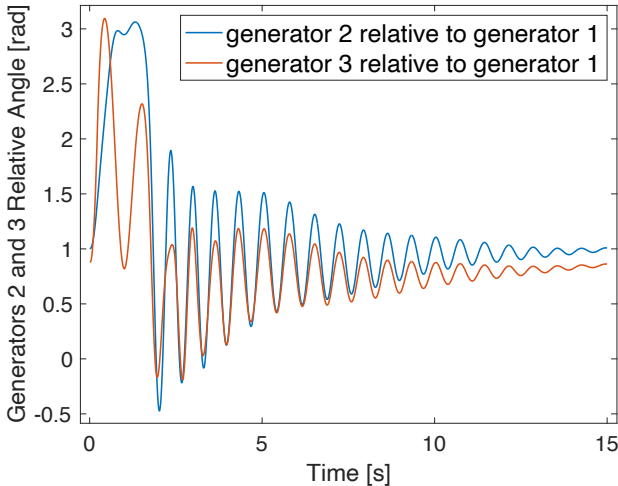


Fig. 8. The angle of generator two and generator three relative to generator one in the one-dimensional parameter space, where the moment of inertia scaling factor is the parameter of interest, at $p = p^* \left(\frac{1}{60}\right)$.

For the multi-dimensional parameter space, we consider the parameter set consisting of the moment of inertia of each of the three generators, the real and reactive load voltage exponents for each of the three loads, the AVR and PSS controller gains

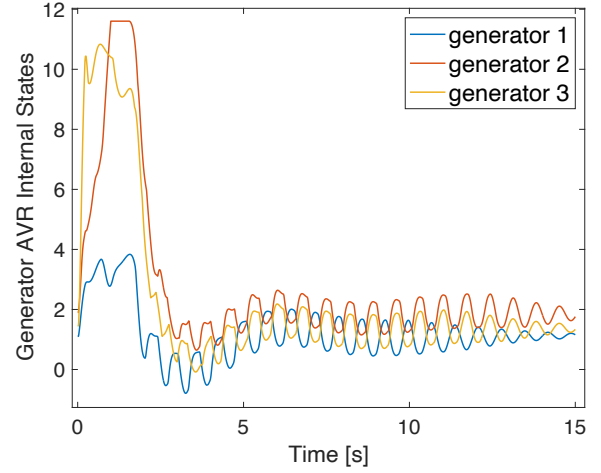


Fig. 9. The internal state dynamics of the AVR of all three synchronous generators in the one-dimensional parameter space, where the moment of inertia scaling factor is the parameter of interest, at $p = p^* \left(\frac{1}{60}\right)$.

for each of the three generators (15 parameters). This set captures both the uncertainty in load dynamic characteristics and the influence of controller response on system recoverability. Let H_1 , H_2 , and H_3 be the moment of inertia of generator one, generator two, and generator three, respectively. Let e_1 , e_2 , and e_3 be the real load voltage exponents for each of the three loads. Let e_4 , e_5 , and e_6 be the reactive load voltage exponents for each of the three loads. Let K_1 , K_2 , and K_3 be the AVR controller gains of generator one, generator two, and generator three, respectively. Let L_1 , L_2 , and L_3 be the PSS controller gains of generator one, generator two, and generator three, respectively. Let $H = [H_1 \ H_2 \ H_3]^T$, $e = [e_1 \ e_2 \ e_3 \ e_4 \ e_5 \ e_6]^T$, $K = [K_1 \ K_2 \ K_3]^T$, and $L = [L_1 \ L_2 \ L_3]^T$. Let $p = [H \ e \ K \ L]^T$ be the vector of chosen parameters. Let p_0 be the initial parameter values, as given in Table II. We apply the optimization approach [14] to find the closest point on the recovery boundary to the nominal value of this 15-dimensional parameter space, with the solution tolerance set to $\epsilon = 10^{-5}$.

H_1	H_2	H_3	e_1	e_2
$\frac{23.64}{60\pi}$	$\frac{6.4}{60\pi}$	$\frac{3.01}{60\pi}$	2	2
e_3	e_4	e_5	e_6	K_1
2	2	2	2	20
K_2	K_3	L_1	L_2	L_3
20	20	$\frac{0.5}{120\pi}$	$\frac{0.5}{120\pi}$	$\frac{0.5}{120\pi}$

TABLE II
TEST CASE PARAMETER VALUES.

The parameter value on the recovery boundary $p^* \left(\frac{1}{60}\right) = [H^* \ e^* \ K^* \ L^*]^T$ for this 15-dimensional parameter space is shown in Table III, which closely approximates the exact theoretical boundary value, and is arbitrarily close to the initial parameter value. Since the location of the CUEP is unknown, we are unable to determine $A \left(p^* \left(\frac{1}{60}\right)\right)$ and, consequently, $v \left(p^* \left(\frac{1}{60}\right)\right)$ directly. Instead, we set $\hat{p} = p^* \left(\frac{1}{60}\right)$ once again and numerically compute $\tilde{F}(\hat{p})$.

Consistent with Theorem 4, $\tilde{F}(\hat{p})$ possesses a unique un-

H_1^*	H_2^*	H_3^*	e_1^*	e_2^*
0.1254	0.0340	0.0160	2	2
e_3^*	e_4^*	e_5^*	e_6^*	K_1^*
2	2	2	2	20
K_2^*	K_3^*	L_1^*	L_2^*	L_3^*
20	20	0.0013	0.0013	0.0013

TABLE III

CLOSEST BOUNDARY PARAMETER VALUE FOR MOMENT OF INERTIA, REAL AND REACTIVE LOAD VOLTAGE EXPONENTS, AVR AND PSS CONTROLLER GAINS.

stable eigenvalue and, by Theorem 4, its associated unstable eigenvector is a close approximation to the mode of instability. Table IV presents the components of $\tilde{v}(p^*(\frac{1}{60}))$ apart from those that are close to zero. The components of $\omega_1, \omega_2, \omega_3, \theta_1, \theta_2, \theta_3, x_1, x_2, x_3$ of $\tilde{v}(\hat{p})$ carry the same interpretation as those in the one-dimensional parameter space.

ω_1	ω_2	ω_3
0.1106	0.4388	0.6850
θ_1	θ_2	θ_3
0.0300	0.1192	0.1861
x_1	x_2	x_3
0.1150	0.2648	0.4267

TABLE IV

COMPONENTS OF $\tilde{v}(\hat{p})$ REPRESENTING THE FREQUENCIES ω , ANGLES θ , AND THE INTERNAL STATE OF THE AVR x FOR THE THREE SYNCHRONOUS GENERATORS IN THE CASE OF 15-DIMENSIONAL PARAMETER SPACE.

Unlike the one-dimensional case with the moment of inertia scaling factor, for the given higher dimensional parameter space, generator three has the largest frequency, angle, and the AVR internal state components in magnitude, followed by generator two and then generator one. This provides a clear indication that generator three plays the most significant role in the failure to recover from the disturbance, which is intuitive since the disturbance originates near generator three, followed by generator two and then generator one. To further validate this observation, the frequency dynamics of all three generators before they reach synchronism, and the angle of generator three and generator two relative to generator one as a function of time, are shown in Fig. 10 and Fig. 11, respectively. We observe that after the fault is cleared, the frequency of generator three exhibits a long transient, with large oscillations starting earlier and ending later than for the other generators, with generator two having the second largest initial frequency transient, and finally generator one having the smallest. Furthermore, the relative angle of generator three has greater amplitude oscillations than those of generator two. Fig. 12 illustrates the AVR internal state dynamics for all three generators. We can see that the internal state of the AVR of generator three has a larger initial transient than the internal state of the AVR of generator two, and generator one has the smallest initial transient in its AVR internal state. All of these observations highlight that the frequency and angle dynamics of generator three, along with the operation of its AVR, are the primary factors influencing whether the system can recover from the disturbance, followed by those of generator two, and then of generator one. Notably and non-intuitively, although both the frequency and voltage dynamics play a major role

in the mechanism of instability in this case, the dynamics of the PSS, which are designed to limit the coupling between frequency and voltage dynamics, do not play a significant role in the failure to recover.

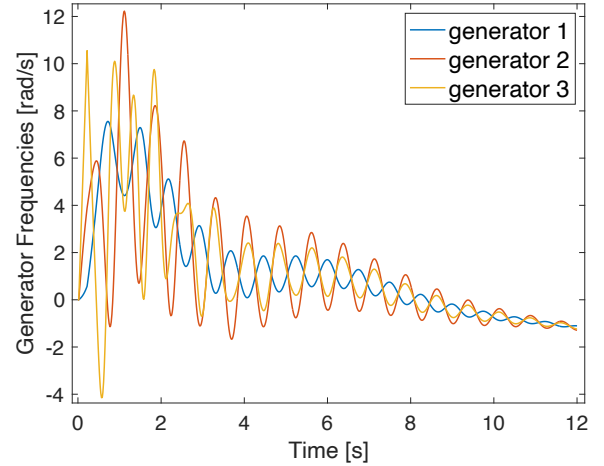


Fig. 10. The frequency dynamics of all three generators before reaching synchronism in the 15-dimensional parameter space, where the parameters of interest are the moment of inertia, real and reactive load voltage exponents, AVR and PSS controller gains, at $p = p^*(\frac{1}{60})$.

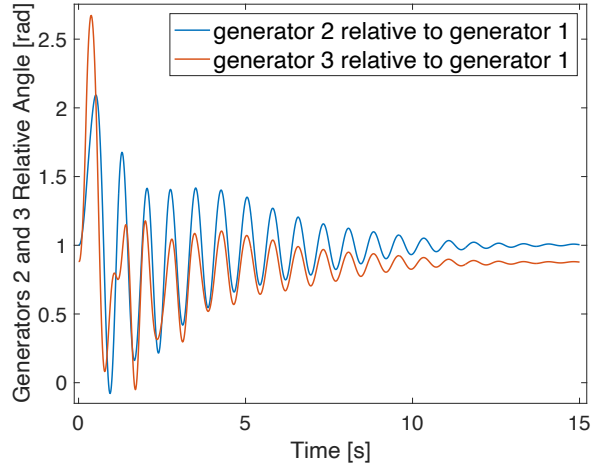


Fig. 11. The angle of generator two and generator three relative to generator one in the 15-dimensional parameter space, where the parameters of interest are the moment of inertia, real and reactive load voltage exponents, AVR and PSS controller gains, at $p = p^*(\frac{1}{60})$.

Overall, the proposed algorithm was successfully applied to the IEEE 9-bus benchmark power system to compute the nonlinear mode of instability for both one-dimensional and higher dimensional parameter spaces, and revealed unexpected dynamic behavior responsible for the mechanism of instability that would not have been straightforward to identify otherwise.

V. PROOFS

Proof of Theorem 1. This proof proceeds by splitting the system trajectory for $p \in R$ with p near p^* into three segments as illustrated in Fig. 13: (i) a segment that starts from the IC $x_0(p)$ and enters a ball N around the CUEP, (ii) another

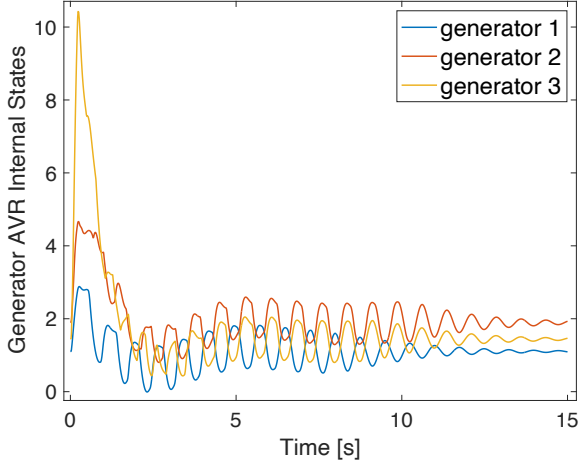


Fig. 12. The internal state dynamics of the AVR of all three synchronous generators in the 15-dimensional parameter space, where the parameters of interest are the moment of inertia, real and reactive load voltage exponents, AVR and PSS controller gains, at $p = p^* (\frac{1}{60})$.

segment that travels within N , and (iii) a final segment that leaves N and enters the local stable manifold of the SEP. The key idea is that as p approaches p^* , the system trajectory spends only a finite amount of time on segments (i) and (iii), but the amount of time it spends in segment (ii) diverges towards infinity. Thus, the value of the Jacobian along segment (ii), which is very close to the Jacobian at the CUEP, will dominate in the calculation of the average $F(p)$ as p approaches p^* .

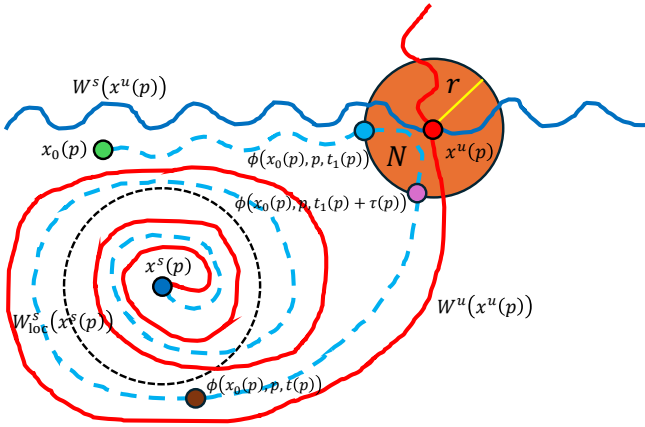


Fig. 13. The system trajectory (cyan dashed line) for parameter values near the recovery boundary from the IC $x_0(p)$ (green circle) and converges to the SEP $x^s(p)$ (dark blue circle). The stable manifold $W^s(x^u(p))$ (blue solid line) and the unstable manifold of $W^u(x^u(p))$ (red solid line) of the CUEP $x^u(p)$ (red circle), are shown.

Let $\epsilon > 0$. To show that $\lim_{p \rightarrow p^*} F(p) = A(p^*)$, it suffices to show that there exists $\delta > 0$ such that $\|p - p^*\| < \delta$ with $p \in R$ implies that $\|F(p) - A(p^*)\| < \epsilon$. Let p^* be the unique closest boundary parameter value to p_0 as in Proposition 2, and let $x^u(p^*)$ be the CUEP. Then, by [12, Corollary 4.28], $\lim_{t \rightarrow \infty} \phi(x_0(p^*), p^*, t) = x^u(p^*)$. Since f is C^1 its first derivatives are continuous, so this implies that

$\lim_{t \rightarrow \infty} \frac{\partial f}{\partial x}(\phi(x_0(p^*), p^*, t)) = \frac{\partial f}{\partial x}(x^u(p^*)) = A(p^*)$. As f is C^1 at $(x^u(p^*), p^*)$, there exist $\delta > 0$ and $r > 0$ such that whenever $\|p - p^*\| < \delta$ and $\|x - x^u(p^*)\| < r$,

$$\left\| \frac{\partial f}{\partial x}(x, p) - A(p^*) \right\| < \frac{\epsilon}{3}. \quad (18)$$

Let $N = B_r(x^u(p^*))$ denote the closed ball of radius r centered at $x^u(p^*)$. Consider the system trajectory for $p = p^*$. As $\lim_{t \rightarrow \infty} \phi(x_0(p^*), p^*, t) = x^u(p^*) \in N$, there exists some finite time at which $\phi(x_0(p^*), p^*, t) \in \partial N$. Shrink r if necessary such that for $p = p^*$ the system trajectory intersects ∂N transversely at the final time $\hat{t}_1 > 0$ at which it passes inwards through ∂N , and such that ∂N is transverse to the local unstable manifold $W_{loc}^u(x^u(p^*))$ with a single point of intersection inside $W^s(x^s(p^*))$.

Define the C^1 function

$$\begin{aligned} \Phi(p, t) &:= \\ &[\phi(x_0(p), p, t) - x^u(p)]^\top [\phi(x_0(p), p, t) - x^u(p)] - r^2. \end{aligned}$$

As $\phi(x_0(p^*), p^*, \hat{t}_1) \in \partial N = \partial B_r(x^u(p^*))$, $\Phi(p^*, \hat{t}_1) = 0$. Furthermore, $\frac{\partial \Phi}{\partial t}(p^*, \hat{t}_1) \neq 0$ (i.e., is full rank) because of the transversal intersection between the system trajectory at $p = p^*$ and ∂N . By the implicit function theorem [21, Theorem C.40], there exist open neighborhoods $V_0 \subseteq \mathbb{R}^m$ of p^* , $W_0 \subseteq \mathbb{R}$ of \hat{t}_1 , and a C^1 function $t_1 : V_0 \rightarrow W_0$ such that $\Phi(p, t) = 0$ for $(p, t) \in V_0 \times W_0$ if and only if $t = t_1(p)$. This gives $\hat{t}_1 = t_1(p^*)$ so that $\lim_{p \rightarrow p^*} t_1(p) = t_1(p^*) = \hat{t}_1$. Shrink δ if necessary such that whenever $\|p - p^*\| < \delta$,

$$|t_1(p) - \hat{t}_1| < \epsilon. \quad (19)$$

For $p \in R$ with $\|p - p^*\| < \delta$, define $\tau(p)$ such that $t_1(p) + \tau(p)$ is the final time at which the system trajectory passes outwards through ∂N . Note that this is finite and well-defined since $\lim_{t \rightarrow \infty} \phi(x_0(p), p, t) = x^s(p) \notin \bar{N}$ and there exists at least one inward crossing of ∂N at $t_1(p)$. Let $x_2(p) = \phi(x_0(p), p, t_1(p) + \tau(p))$. By [12, Theorem 4.32], $\lim_{p \rightarrow p^*} \tau(p) = \infty$.

Let \hat{x}_2 be the single point of transversal intersection between $W_{loc}^u(x^u(p^*))$ and ∂N in $W^s(x^s(p^*))$. We next show that $\lim_{p \rightarrow p^*} x_2(p) = \hat{x}_2$. So, let $\tilde{\epsilon} > 0$. As $W_{loc}^u(x^u(p^*))$ and ∂N are compact and have a single point of transversal intersection in $W^s(x^s(p^*))$, there exists $\hat{\epsilon} > 0$ such that for any manifold M that satisfies $d_{C_1}(M, W_{loc}^u(x^u(p^*))) < \hat{\epsilon}$, M intersects N transversely with a single point of intersection in $W^s(x^s(p^*))$ and $d_{C_1}(M \cap \partial N \cap W^s(x^s(p^*)), \hat{x}_2) < \tilde{\epsilon}$ [17, Corollary A.3.18]. Note that $M \cap \partial N \cap W^s(x^s(p^*))$ is this single point of intersection.

Consider $B_\delta(p^*)$, the open ball of radius δ centered at p^* . Let $\phi(x_0(B_\delta(p^*)), p, t) := \cup_{p \in B_\delta(p^*)} \phi(x_0(p), p, t)$, and note that $x_0(B_\delta(p^*))$ is a C^1 manifold that is transverse to $W^s(x^u(p^*))$ by Proposition 1(ii). Thus, by the Inclination Lemma [22], shrinking δ further if necessary, there exists $T > 0$ such that whenever $p \in B_\delta(p^*)$ and $t > T$,

$$d_{C_1}(\phi(x_0(B_\delta(p^*)), p, t) \cap N, W_{loc}^u(x^u(p))) < \frac{\hat{\epsilon}}{2}, \quad (20)$$

where $\phi(x_0(B_\delta(p^*)), p, t) \cap N$ refers to the connected component of this intersection that contains

$\phi(x_0(p^*), p^*, t)$. Since $W_{\text{loc}}^u(x^u(p))$ is continuous in p , $\lim_{p \rightarrow p^*} W_{\text{loc}}^u(x^u(p)) = W_{\text{loc}}^u(x^u(p^*))$. Shrink δ if necessary such that whenever $\|p - p^*\| < \delta$,

$$d_{C_1}(W_{\text{loc}}^u(x^u(p)), W_{\text{loc}}^u(x^u(p^*))) < \frac{\hat{\epsilon}}{2}. \quad (21)$$

Thus, we have

$$\begin{aligned} & d_{C_1}(\phi(x_0(B_\delta(p^*)), p, t) \cap N, W_{\text{loc}}^u(x^u(p^*))) \\ & \stackrel{\text{triangle inequality}}{\leq} d_{C_1}(\phi(x_0(B_\delta(p^*)), p, t) \cap N, W_{\text{loc}}^u(x^u(p))) \\ & + d_{C_1}(W_{\text{loc}}^u(x^u(p)), W_{\text{loc}}^u(x^u(p^*))) \\ & \stackrel{(20), (21)}{<} \frac{\hat{\epsilon}}{2} + \frac{\hat{\epsilon}}{2} = \hat{\epsilon}. \end{aligned}$$

By the above, this implies that for any $\|p - p^*\| < \delta$ and $t > T$, $\phi(x_0(B_\delta(p^*)), p, t)$ is transverse to ∂N with a single point of intersection in $W^s(x^s(p^*))$, and that $d_{C_1}(\phi(x_0(B_\delta(p^*)), p, t) \cap \partial N \cap W^s(x^s(p^*)), \hat{x}_2) < \tilde{\epsilon}$. Since $\lim_{p \rightarrow p^*} t_1(p) + \tau(p) = \infty$, shrink δ if necessary such that whenever $\|p - p^*\| < \delta$, $t_1(p) + \tau(p) > T$. As $x_2(p) = \phi(x_0(p), p, t_1(p) + \tau(p)) \in \partial N$ and $\phi(x_0(B_\delta(p^*)), p, t_1(p) + \tau(p))$ has a single point of intersection with ∂N in $W^s(x^s(p^*))$, it must hold that $x_2(p)$ is this single point of intersection. Thus, we have

$$\begin{aligned} & d_{C_1}(x_2(p), \hat{x}_2) = \\ & d_{C_1}(\phi(x_0(B_\delta(p^*)), p, t_1(p) + \tau(p)) \cap \partial N \cap W^s(x^s(p^*)), \hat{x}_2) < \tilde{\epsilon}. \end{aligned}$$

Since $\tilde{\epsilon} > 0$ was arbitrary, this proves $\lim_{p \rightarrow p^*} x_2(p) = \hat{x}_2$.

Next, consider the system trajectory at time t starting from the initial condition \hat{x}_2 , denoted by $\phi(\hat{x}_2, p^*, t)$. As $\hat{x}_2 \in W^s(x^s(p^*))$, there exists $\hat{t}_2 > 0$ such that $\phi(\hat{x}_2, p^*, \hat{t}_2) \in \text{int } W_{\text{loc}}^s(x^s(p^*))$. As $W_{\text{loc}}^s(x^s(p))$ varies continuously with p , $\lim_{p \rightarrow p^*} x_2(p) = \hat{x}_2$, and the flow is continuous, shrinking δ further if necessary implies that for $\|p - p^*\| < \delta$, $\phi(x_2(p), p, \hat{t}_2) \in \text{int } W_{\text{loc}}^s(x^s(p))$. Recall that for all $\|p - p^*\| < \delta$, $W_{\text{loc}}^s(x^s(p))$ is forward invariant and has $\frac{\partial f}{\partial x}(x)$ stable for all $x \in W_{\text{loc}}^s(x^s(p))$. Thus, for all $\|p - p^*\| < \delta$ and $t \geq \hat{t}_2$, $\frac{\partial f}{\partial x}(\phi(x_2(p), p, t))$ is stable. For $p \in R$, as $t(p)$ is the supremum over time at which $\frac{\partial f}{\partial x}(\phi(x_0(p), p, t))$ is unstable, this implies that

$$t(p) < t_1(p) + \tau(p) + \hat{t}_2 \quad (22)$$

for all $\|p - p^*\| < \delta$.

For $\|p - p^*\| < \delta$ with $p \in R$, define the functions

$$\Psi(p) := \sup_{t \in [0, t_1(p)]} \left\| \frac{\partial f}{\partial x}(\phi(x_0(p), p, t)) - A(p^*) \right\|, \quad (23)$$

$$\hat{\Psi}(p) := \sup_{t \in [0, \hat{t}_2]} \left\| \frac{\partial f}{\partial x}(\phi(x_2(p), p, t)) - A(p^*) \right\|. \quad (24)$$

As f and the flow are C^1 , $x_0(p)$ and $x_2(p)$ are continuous at p^* , the norm is continuous, so $\left\| \frac{\partial f}{\partial x}(\phi(x_0(p), p, t)) - A(p^*) \right\|$ and $\left\| \frac{\partial f}{\partial x}(\phi(x_2(p), p, t)) - A(p^*) \right\|$ are both continuous in (p, t) . Thus, as $[0, t_1(p)]$ and $[0, \hat{t}_2]$ are compact, nonempty, and continuous in p (since $t_1(p)$ is continuous), by the

maximum theorem [23, Page 116], Ψ and $\hat{\Psi}$ are continuous at p^* . Thus,

$$\begin{aligned} \lim_{p \rightarrow p^*} \Psi(p) &= \lim_{p \rightarrow p^*} \sup_{t \in [0, t_1(p)]} \left\| \frac{\partial f}{\partial x}(\phi(x_0(p), p, t)) - A(p^*) \right\| \\ &= \sup_{t \in [0, \hat{t}_1]} \left\| \frac{\partial f}{\partial x}(\phi(x_0(p^*), p^*, t)) - A(p^*) \right\| \\ &=: \Psi(p^*) \end{aligned} \quad (25)$$

and

$$\begin{aligned} \lim_{p \rightarrow p^*} \hat{\Psi}(p) &= \lim_{p \rightarrow p^*} \sup_{t \in [0, \hat{t}_2]} \left\| \frac{\partial f}{\partial x}(\phi(x_2(p), p, t)) - A(p^*) \right\| \\ &= \sup_{t \in [0, \hat{t}_2]} \left\| \frac{\partial f}{\partial x}(\phi(\hat{x}_2, p^*, t)) - A(p^*) \right\| \\ &=: \hat{\Psi}(p^*). \end{aligned} \quad (26)$$

Since $t(p) > \tau(p) + t_1(p)$ and $\lim_{p \rightarrow p^*} \tau(p) = \infty$, $\lim_{p \rightarrow p^*} t(p) = \infty$. Thus, shrink δ further if necessary such that whenever $\|p - p^*\| < \delta$,

$$t(p) > \frac{3(\hat{t}_1 + \epsilon)(\Psi(p^*) + \epsilon)}{\epsilon}, \quad (27)$$

$$t(p) > \frac{3\hat{t}_2(\hat{\Psi}(p^*) + \epsilon)}{\epsilon}, \quad (28)$$

$$|\Psi(p) - \Psi(p^*)| < \epsilon, \quad (29)$$

$$|\hat{\Psi}(p) - \hat{\Psi}(p^*)| < \epsilon, \quad (30)$$

where the final two equations follow from (25)-(26).

By the definitions of Ψ and $\hat{\Psi}$ in (23) and (24), we also have that for $t \in [0, t_1(p)]$, $\left\| \frac{\partial f}{\partial x}(\phi(x_0(p), p, t)) - A(p^*) \right\| \leq \Psi(p)$, and for $t \in [0, \hat{t}_2]$, $\left\| \frac{\partial f}{\partial x}(\phi(x_2(p), p, t)) - A(p^*) \right\| \leq \hat{\Psi}(p)$. Thus, for any $\|p - p^*\| < \delta$, we have

$$\begin{aligned} & \|F(p) - A(p^*)\| \\ &= \left\| \frac{1}{t(p)} \int_0^{t(p)} \frac{\partial f}{\partial x}(\phi(x_0(p), p, t)) dt - A(p^*) \right\| \\ &= \left\| \frac{1}{t(p)} \int_0^{t(p)} \left[\frac{\partial f}{\partial x}(\phi(x_0(p), p, t)) - A(p^*) \right] dt \right\| \\ &\leq \frac{1}{t(p)} \int_0^{t(p)} \left\| \frac{\partial f}{\partial x}(\phi(x_0(p), p, t)) - A(p^*) \right\| dt \\ &= \frac{1}{t(p)} \left[\int_0^{t_1(p)} \left\| \frac{\partial f}{\partial x}(\phi(x_0(p), p, t)) - A(p^*) \right\| dt \right. \\ &\quad + \int_{t_1(p)}^{t_1(p)+\tau(p)} \left\| \frac{\partial f}{\partial x}(\phi(x_0(p), p, t)) - A(p^*) \right\| dt \\ &\quad \left. + \int_{t_1(p)+\tau(p)}^{t(p)} \left\| \frac{\partial f}{\partial x}(\phi(x_0(p), p, t)) - A(p^*) \right\| dt \right] \\ &\stackrel{(22)}{<} \frac{1}{t(p)} \left[\int_0^{t_1(p)} \left\| \frac{\partial f}{\partial x}(\phi(x_0(p), p, t)) - A(p^*) \right\| dt \right. \\ &\quad \left. + \int_{t_1(p)}^{t_1(p)+\tau(p)} \left\| \frac{\partial f}{\partial x}(\phi(x_0(p), p, t)) - A(p^*) \right\| dt \right] \end{aligned}$$

$$\begin{aligned}
& + \int_{t_1(p)+\tau(p)}^{t_1(p)+\tau(p)+\hat{t}_2} \left\| \frac{\partial f}{\partial x} (\phi(x_0(p), p, t)) - A(p^*) \right\| dt \Big] \\
& = \frac{1}{t(p)} \left[\int_0^{t_1(p)} \left\| \frac{\partial f}{\partial x} (\phi(x_0(p), p, t)) - A(p^*) \right\| dt \right. \\
& + \int_{t_1(p)}^{t_1(p)+\tau(p)} \left\| \frac{\partial f}{\partial x} (\phi(x_0(p), p, t)) - A(p^*) \right\| dt \\
& + \left. \int_0^{\hat{t}_2} \left\| \frac{\partial f}{\partial x} (\phi(x_2(p), p, t)) - A(p^*) \right\| dt \right] \\
& \stackrel{(18),(23),(24)}{<} \frac{1}{t(p)} \left[\int_0^{t_1(p)} \Psi(p) dt + \int_{t_1(p)}^{t_1(p)+\tau(p)} \frac{\epsilon}{3} dt \right. \\
& + \left. \int_0^{\hat{t}_2} \hat{\Psi}(p) dt \right] \\
& = \frac{t_1(p) \Psi(p)}{t(p)} + \frac{\tau(p) \epsilon}{t(p) 3} + \frac{\hat{t}_2 \hat{\Psi}(p)}{t(p)} \\
& \stackrel{(19),(29),(30)}{<} \frac{(\hat{t}_1 + \epsilon) (\Psi(p^*) + \epsilon)}{t(p)} + \frac{\epsilon}{3} + \frac{\hat{t}_2 (\hat{\Psi}(p^*) + \epsilon)}{t(p)} \\
& \stackrel{(27),(28)}{<} \frac{(\hat{t}_1 + \epsilon) (\Psi(p^*) + \epsilon)}{\frac{3(\hat{t}_1 + \epsilon) (\Psi(p^*) + \epsilon)}{\epsilon}} + \frac{\epsilon}{3} + \frac{\hat{t}_2 (\hat{\Psi}(p^*) + \epsilon)}{\frac{3\hat{t}_2 (\hat{\Psi}(p^*) + \epsilon)}{\epsilon}} \\
& = \frac{\epsilon}{3} + \frac{\epsilon}{3} + \frac{\epsilon}{3} = \epsilon,
\end{aligned}$$

so $\|F(p) - A(p^*)\| < \epsilon$ for all $\|p - p^*\| < \delta$ with $p \in R$, which completes the proof of Theorem 1. \square

Proof of Theorem 2. Recall that $\lambda(p^*)$ is the simple unstable eigenvalue of $A(p^*)$ and $v(p^*)$ is its corresponding eigenvector. Furthermore, $A(p^*)$ is hyperbolic by Proposition 1 and its proof, so all eigenvalues of $A(p^*)$ other than $\lambda(p^*)$ are stable (i.e., no eigenvalues of $A(p^*)$ have zero real part). Since the eigenvalues of a matrix are continuous functions of the elements of that matrix [24, Theorem 3.1.2], and by Theorem 1 $\lim_{p \rightarrow p^*} F(p) = A(p^*)$, this implies that the eigenvalues of $F(p)$ converge to the eigenvalues of $A(p^*)$ in the limit as $p \rightarrow p^*$. Thus, there exists $\delta > 0$ sufficiently small such that $\|p - p^*\| < \delta$ implies that $F(p)$ is hyperbolic and has exactly one unstable eigenvalue, call it $\lambda(p)$. Let $v(p)$ denote the eigenvector associated with $\lambda(p)$. As the eigenvalues of $F(p)$ converge to those of $A(p^*)$ in the limit as $p \rightarrow p^*$, $\lambda(p)$ is the unique unstable eigenvalue of $F(p)$, and $\lambda(p^*)$ is the unique unstable eigenvalue of $A(p^*)$, this implies that $\lim_{p \rightarrow p^*} \lambda(p) = \lambda(p^*)$. Since $\lambda(p)$ is a simple (i.e., multiplicity one) eigenvalue of $F(p)$ and $v(p)$ is its associated eigenvector, and since $\lim_{p \rightarrow p^*} F(p) = A(p^*)$, by [24, Theorem 3.1.3] $\lim_{p \rightarrow p^*} v(p) = v(p^*)$. This completes the proof of Theorem 2. \square

Proof of Theorem 3. The goal of this proof is to follow a similar argument as in the proof of Theorem 1, which involves splitting the system trajectory for $p \in R$ with p close to p^* into three segments as illustrated in Fig. 14. Recall the definition of $j(p)$ from (9). We begin by showing that $\lim_{p \rightarrow p^*} j(p) = \infty$. Let $K > 0$. As

$\lim_{n \rightarrow \infty} T^n(x_0(p^*), p^*, h) = x^u(p^*)$, $\frac{\partial f}{\partial x}(x^u(p^*)) = A(p^*)$ is unstable and hyperbolic, and $\frac{\partial f}{\partial x}$ is continuous, there exists $i \in \mathbb{N}$ such that $ih > K$ and $\frac{\partial f}{\partial x}(T^i(x_0(p^*), p^*, h))$ is unstable. Since $\frac{\partial f}{\partial x}(T^i(x_0(p), p, h))$ is continuous in p , there exists $\delta > 0$ such that whenever $\|p - p^*\| < \delta$, $\frac{\partial f}{\partial x}(T^i(x_0(p), p, h))$ is unstable. Hence, by the definition of $j(p)$ in (9), $j(p) \geq ih > K$. As K was arbitrary, this implies that $\lim_{p \rightarrow p^*} j(p) = \infty$.

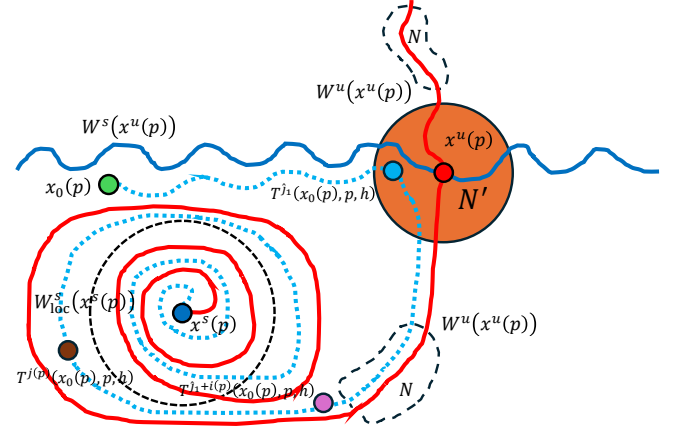


Fig. 14. The system trajectory in discrete time (cyan dotted line) for parameter values near the recovery boundary. This figure is similar to Fig. 13, except we are considering the state obtained from the continuous time system (1)-(2) with new labels and definitions.

As in the proof of Theorem 1, there exist $r > 0$ and $\delta > 0$ such that whenever $\|p - p^*\| < \delta$ and $\|x - x^u(p^*)\| < r$,

$$\left\| \frac{\partial f}{\partial x}(x, p) - A(p^*) \right\| < \frac{\epsilon}{3}. \quad (31)$$

Shrink r further so that (31) holds for some $r' > r$. As in the proof of Theorem 1, shrink r further if necessary such that $\partial B_{r'}(x^u(p^*))$ is transverse to the local unstable manifold $W^u_{loc}(x^u(p^*))$ with a single point of intersection \hat{x}_2 inside $W^s(x^s(p^*))$ and a single point of intersection \tilde{x}_2 outside $W^s(x^s(p^*))$. Let $\hat{x}_1 = T^{-1}(\hat{x}_2, p^*, h)$ and $\tilde{x}_1 = T^{-1}(\tilde{x}_2, p^*, h)$. Since $W^u(x^u(p^*))$ is one-dimensional, let \hat{D} be the subset of $W^u(x^u(p^*))$ from \hat{x}_1 to \hat{x}_2 , \tilde{D} be the subset of $W^u(x^u(p^*))$ from \tilde{x}_1 to \tilde{x}_2 , and $D = \hat{D} \cup \tilde{D}$. Then by [11, Lemma 5.4] (or, similarly, from the proof of [22, Theorem 1.9]), shrinking δ further if necessary implies that there exist open neighborhoods N and N' such that $D \subset N$, \bar{N} is disjoint from $W^s(x^u(p^*))$ and $\partial W^s(x^s(p^*))$, $\bar{N} \subset B_{r'}(x^u(p^*))$, \bar{N} is compact, and for $\|p - p^*\| < \delta$, N' contains $x^u(p)$ and $\bigcup_{i=0}^{\infty} T^{-i}(N, p, h) \cup W^s(x^u(p))$ contains N' [12, Lemma 5.1]. Let $\hat{N} = (N' \cup N) \cap B_{r'}(x^u(p^*))$, and note that $N \subset \hat{N}$.

Let \hat{j}_1 be the final time index at which $T^n(x_0(p^*), p^*, h)$ enters the interior of \hat{N} . Since $T^{\hat{j}_1}(x_0(p), p, h)$ is continuous in p , shrink δ if necessary such that whenever $\|p - p^*\| < \delta$, $T^{\hat{j}_1}(x_0(p), p, h)$ enters the interior of \hat{N} . For $p \in R$ with $\|p - p^*\| < \delta$, define $i(p)$ such that $\hat{j}_1 + i(p)$ is the final time index at which $T^n(x_0(p), p, h)$ exits N , and let $x_2(p) = T^{\hat{j}_1 + i(p)}(x_0(p), p, h)$. Note that $i(p)$ is well-defined since for $p \in R$ with $\|p - p^*\| < \delta$, $T^{\hat{j}_1}(x_0(p), p, h) \in \hat{N}$, so since $T^{\hat{j}_1}(x_0(p), p, h)$ is not in $W^s(x^u(p))$, it must be

in $T^{-i}(N, p, h)$ for some positive integer i . This implies that $T^{\hat{j}_1+n}(x_0(p), p, h)$ must pass through N after a finite number of time steps, before ultimately converging to $x^s(p)$. Let $S = \bar{N} \cap \bar{W}^s(x^s(p^*))$, which is compact. Then $S \subset W^s(x^s(p^*))$ since \bar{N} and $\partial W^s(x^s(p^*))$ are disjoint. Then as S is compact and T^n is continuous, there exists a time index \hat{j}_2 sufficiently large such that $T^{\hat{j}_2}(S, p^*, h) \subset \text{int } W_{\text{loc}}^s(x^s(p^*))$. As $W_{\text{loc}}^s(x^s(p))$ is continuous in p , S is compact, and $T^{\hat{j}_2}$ is continuous, shrink δ further if necessary such that $\|p - p^*\| < \delta$ with $p \in R$ implies that $T^{\hat{j}_2}(S, p, h) \subset \text{int } W_{\text{loc}}^s(x^s(p))$. As $\text{int } W_{\text{loc}}^s(x^s(p))$ is forward invariant and the Jacobian is stable for each $x \in W_{\text{loc}}^s(x^s(p))$, this implies that for $p \in R$ with $\|p - p^*\| < \delta$,

$$j(p) < \hat{j}_1 + i(p) + \hat{j}_2. \quad (32)$$

For $p \in R$ with $\|p - p^*\| < \delta$, define the functions

$$\Psi(p) := \max_{n \in \{0, \dots, \hat{j}_1-1\}} \left\| \frac{\partial f}{\partial x}(T^n(x_0(p), p, h)) - A(p^*) \right\|, \quad (33)$$

$$\hat{\Psi}(p) := \max_{n \in \{0, \dots, \hat{j}_2\}} \left\| \frac{\partial f}{\partial x}(T^n(x_2(p), p, h)) - A(p^*) \right\|. \quad (34)$$

Note that $\Psi(p)$ and $\hat{\Psi}(p)$, as the maximums of a finite number of continuous functions, are themselves continuous. We have

$$\begin{aligned} \lim_{p \rightarrow p^*} \Psi(p) &= \Psi(p^*) \\ &:= \max_{n \in \{0, \dots, \hat{j}_1-1\}} \left\| \frac{\partial f}{\partial x}(T^n(x_0(p^*), p^*, h)) - A(p^*) \right\|. \end{aligned}$$

As $\max_{n \in \{0, \dots, \hat{j}_2\}} \left\| \frac{\partial f}{\partial x}(T^n(x_2(p), p, h)) - A(p^*) \right\|$ is continuous, $x_2(p) \in N$, and \bar{N} is compact,

$$\begin{aligned} \hat{\Psi}(p) &\leq \sup_{x \in \bar{N}} \max_{n \in \{0, \dots, \hat{j}_2\}} \left\| \frac{\partial f}{\partial x}(T^n(x, p, h)) - A(p^*) \right\| \\ &=: \hat{\Psi}(p^*) < \infty. \end{aligned} \quad (35)$$

Since $\lim_{p \rightarrow p^*} j(p) = \infty$, shrink δ if necessary such that whenever $p \in R$ with $\|p - p^*\| < \delta$,

$$j(p) > \frac{3\hat{j}_1(\Psi(p^*) + \epsilon)}{\epsilon}, \quad (36)$$

$$j(p) > \frac{3(\hat{j}_2 + 1)\hat{\Psi}(p^*)}{\epsilon}, \quad (37)$$

$$|\Psi(p) - \Psi(p^*)| < \epsilon. \quad (38)$$

For $n \in \{\hat{j}_1, \dots, \hat{j}_1 + i(p) - 1\}$, since $T^n(x_0(p), p, h) \in B_{r'}(x^u(p^*))$, by (31) we have

$$\left\| \frac{\partial f}{\partial x}(T^n(x_0(p), p, h)) - A(p^*) \right\| < \frac{\epsilon}{3}. \quad (39)$$

Thus, we have whenever $\|p - p^*\| < \delta$,

$$\begin{aligned} &\left\| \hat{F}(p) - A(p^*) \right\| \\ &= \left\| \frac{1}{j(p)} \sum_{n=0}^{j(p)} \frac{\partial f}{\partial x}(T^n(x_0(p), p, h)) - A(p^*) \right\| \end{aligned}$$

$$\begin{aligned} &= \left\| \frac{1}{j(p)} \sum_{n=0}^{j(p)} \left[\frac{\partial f}{\partial x}(T^n(x_0(p), p, h)) - A(p^*) \right] \right\| \\ &\leq \frac{1}{j(p)} \sum_{n=0}^{j(p)} \left\| \frac{\partial f}{\partial x}(T^n(x_0(p), p, h)) - A(p^*) \right\| \\ &= \frac{1}{j(p)} \left[\sum_{n=0}^{\hat{j}_1-1} \left\| \frac{\partial f}{\partial x}(T^n(x_0(p), p, h)) - A(p^*) \right\| \right. \\ &\quad + \sum_{n=\hat{j}_1}^{\hat{j}_1+i(p)-1} \left\| \frac{\partial f}{\partial x}(T^n(x_0(p), p, h)) - A(p^*) \right\| \\ &\quad \left. + \sum_{n=\hat{j}_1+i(p)}^{j(p)} \left\| \frac{\partial f}{\partial x}(T^n(x_0(p), p, h)) - A(p^*) \right\| \right] \\ &\stackrel{(32)}{<} \frac{1}{j(p)} \left[\sum_{n=0}^{\hat{j}_1-1} \left\| \frac{\partial f}{\partial x}(T^n(x_0(p), p, h)) - A(p^*) \right\| \right. \\ &\quad + \sum_{n=\hat{j}_1}^{\hat{j}_1+i(p)-1} \left\| \frac{\partial f}{\partial x}(T^n(x_0(p), p, h)) - A(p^*) \right\| \\ &\quad \left. + \sum_{n=\hat{j}_1+i(p)}^{\hat{j}_1+i(p)+\hat{j}_2} \left\| \frac{\partial f}{\partial x}(T^n(x_0(p), p, h)) - A(p^*) \right\| \right] \\ &= \frac{1}{j(p)} \left[\sum_{n=0}^{\hat{j}_1-1} \left\| \frac{\partial f}{\partial x}(T^n(x_0(p), p, h)) - A(p^*) \right\| \right. \\ &\quad + \sum_{n=\hat{j}_1}^{\hat{j}_1+i(p)-1} \left\| \frac{\partial f}{\partial x}(T^n(x_0(p), p, h)) - A(p^*) \right\| \\ &\quad \left. + \sum_{n=0}^{\hat{j}_2} \left\| \frac{\partial f}{\partial x}(T^n(x_2(p), p, h)) - A(p^*) \right\| \right] \\ &\stackrel{(33),(34),(39)}{<} \frac{1}{j(p)} \left[\sum_{n=0}^{\hat{j}_1-1} \Psi(p) + \sum_{n=\hat{j}_1}^{\hat{j}_1+i(p)-1} \frac{\epsilon}{3} + \sum_{n=0}^{\hat{j}_2} \hat{\Psi}(p) \right] \\ &\stackrel{(35),(38)}{<} \frac{1}{j(p)} \left[\sum_{n=0}^{\hat{j}_1-1} (\Psi(p^*) + \epsilon) + \sum_{n=\hat{j}_1}^{\hat{j}_1+i(p)-1} \frac{\epsilon}{3} \right. \\ &\quad \left. + \sum_{n=0}^{\hat{j}_2} \hat{\Psi}(p^*) \right] \\ &= \frac{\hat{j}_1(\Psi(p^*) + \epsilon)}{j(p)} + \frac{i(p)\epsilon}{j(p)3} + \frac{(\hat{j}_2 + 1)\hat{\Psi}(p^*)}{j(p)} \\ &\stackrel{(36),(37)}{<} \frac{\hat{j}_1(\Psi(p^*) + \epsilon)}{\frac{3\hat{j}_1(\Psi(p^*) + \epsilon)}{\epsilon}} + \frac{\epsilon}{3} + \frac{(\hat{j}_2 + 1)\hat{\Psi}(p^*)}{\frac{3(\hat{j}_2 + 1)\hat{\Psi}(p^*)}{\epsilon}} \\ &= \frac{\epsilon}{3} + \frac{\epsilon}{3} + \frac{\epsilon}{3} = \epsilon, \end{aligned}$$

so $\left\| \hat{F}(p) - A(p^*) \right\| < \epsilon$ for all $\|p - p^*\| < \delta$ with $p \in R$, which completes the proof of (11a). (11b) and (11c) can be proved by following analogous reasoning as in the proof of Theorem 2. This completes the proof of Theorem 3. \square

Proof of Theorem 4. We first prove $\lim_{h \rightarrow 0} p^*(h) = p^*$. Recall that $x_0(p^*) \in W^s(x^u(p^*))$, where $x^u(p^*)$ is the CUEP. Thus, there exists $T > 0$ such that $x_0(p^*) \in \phi(W_{\text{loc}}^s(x^u(p^*)), p^*, -T) \subset \phi(W_{\text{loc}}^s(x^u(J)), J, -T)$. By Assumption 1, $W^s(x^u(J))$ and $x_0(J)$ are transverse, which implies that $\phi(W_{\text{loc}}^s(x^u(J)), J, -T)$ and $x_0(J)$ are transverse, and that $x_0(p^*)$ is a point of their transversal intersection. Then for any $\epsilon > 0$, by [17, Proposition A.3.16] (i.e., the stability of transversal intersections) there exists a $\hat{\delta} > 0$ such that for any manifold M that satisfies $d_{C^1}(M, \phi(W_{\text{loc}}^s(x^u(J)), J, -T)) < \hat{\delta}$, there exists a point $(x, p) \in M \cap x_0(J)$ with $\|(x, p) - (x_0(p^*), p^*)\| < \epsilon$. As $\phi(\cdot, \cdot, -T)$ is C^1 , there exists $\delta > 0$ such that for any manifold M that satisfies $d_{C^1}(M, W_{\text{loc}}^s(x^u(J))) < \delta$, $d_{C^1}(\phi(M, -T), \phi(W_{\text{loc}}^s(x^u(J)), -T)) < \hat{\delta}$, so $\phi(M, -T)$ intersects $x_0(J)$ at a point within an ϵ distance of $(x_0(p^*), p^*)$.

Recall that $T^n(x, p, h) = \phi(x, p, nh)$ for any state x , parameter value p , and time step n . We refer to T as the exact discrete time map with time step h . Let T_d denote the approximation of T that is obtained using numerical integration. Fix some time $\hat{t} > 0$. For any $h > 0$, let $\hat{n}(h)$ be the minimum integer n such that $nh \geq \hat{t}$. Over any compact set $K \times J' \subset \mathbb{R}^n \times J$, define the maps \hat{T} and \hat{T}_d by $\hat{T}(x, p, h) = T^{\hat{n}(h)}(x, p, h)$ and $\hat{T}_d(x, p, h) = T_d^{\hat{n}(h)}(x, p, h)$, respectively, for all $(x, p) \in K \times J'$ and $h > 0$. Then, since the approximation error of the numerical integration approaches zero as $h \rightarrow 0$, we have that $\lim_{h \rightarrow 0} d_{C^1}(\hat{T}_d(\cdot, \cdot, h), \hat{T}(\cdot, \cdot, h)) = 0$. Furthermore, as $\lim_{h \rightarrow 0} h\hat{n}(h) = \hat{t}$, and since \hat{T} represents the exact discrete time map, we also have that $\lim_{h \rightarrow 0} d_{C^1}(\hat{T}(\cdot, \cdot, h), \phi(\cdot, \cdot, \hat{t})) = 0$, where $\phi(\cdot, \cdot, \hat{t})$ is the time- \hat{t} map for the flow ϕ , and is itself a discrete time map. Thus, combining these implies that

$$\lim_{h \rightarrow 0} d_{C^1}(\hat{T}_d(\cdot, \cdot, h), \phi(\cdot, \cdot, \hat{t})) = 0. \quad (40)$$

Note that $x^u(p)$ is a hyperbolic fixed point of $\phi(\cdot, \cdot, \hat{t})$ for all $p \in J$, and that $W_{\text{loc}}^s(x^u(J))$ is its local stable manifold under $\phi(\cdot, \cdot, \hat{t})$, since $\phi(\cdot, \cdot, \hat{t})$ is the exact time- \hat{t} map for the flow ϕ . Thus, there exists $\tilde{\delta} > 0$ such that for any map \tilde{T} with $d_{C^1}(\tilde{T}, \phi(\cdot, \cdot, \hat{t})) < \tilde{\delta}$, \tilde{T} possesses a hyperbolic fixed point \tilde{x}^u near x^u and $d_{C^1}(W_{\text{loc}}^s(\tilde{x}^u(J)), W_{\text{loc}}^s(x^u(J))) < \delta$. By (40), this implies that there exists $\hat{h} > 0$ such that for any $h \in (0, \hat{h})$, $\hat{T}_d(\cdot, \cdot, h)$ possesses a hyperbolic fixed point x_h^u near x^u and $d_{C^1}(W_{\text{loc}}^s(x_h^u(J)), W_{\text{loc}}^s(x^u(J))) < \delta$. Thus, by the above there exists a point $(x_h, p_h) \in W_{\text{loc}}^s(x_h^u(J)) \cap x_0(J)$ with $\|(x_h, p_h) - (x_0(p^*), p^*)\| < \epsilon$. As $\epsilon > 0$ was arbitrary, this implies that the points (x_h, p_h) can be selected such that $\lim_{h \rightarrow 0} p_h = p^*$. Furthermore, as $x_0(p_h) = (x_h, p_h) \in W_{\text{loc}}^s(x_h^u(J))$ for the map $\hat{T}_d(\cdot, \cdot, h)$, $x_0(p_h) \notin W_{\text{loc}}^s(x_h^s(J))$ for this map, where x_h^s represents the SEP of $\hat{T}_d(\cdot, \cdot, h)$ near x^s , so $p_h \notin R$ for this map. Also, x_h^u is a hyperbolic fixed point for both $\hat{T}_d(\cdot, \cdot, h)$ and $T_d(\cdot, \cdot, h)$, and $W_{\text{loc}}^s(x_h^u(J))$ is its local stable manifold under both maps, so $p_h \notin R$ for the map $T_d(\cdot, \cdot, h)$ as well.

Assume towards a contradiction that $\lim_{h \rightarrow 0} p^*(h) \neq p^*$. Then there must exist a monotonically decreasing sequence

$\{h_n\}_{n=1}^{\infty}$ with $\lim_{n \rightarrow \infty} h_n = 0$ such that $\lim_{n \rightarrow \infty} p^*(h_n) \neq p^*$. Since $p^*(h_n)$ is the unique closest parameter value in ∂R to p_0 for the map $T_d(\cdot, \cdot, h_n)$, and since $p_{h_n} \notin R$ for the map $T_d(\cdot, \cdot, h_n)$, for each integer n we have

$$\|p^*(h_n) - p_0\| \leq \|p_{h_n} - p_0\| \leq \sup_{n \geq 1} \|p_{h_n} - p_0\| =: r < \infty,$$

where the supremum is finite since $\lim_{n \rightarrow \infty} p_{h_n} = p^*$. Therefore, the sequence $\{p^*(h_n)\}_{n=1}^{\infty}$ is contained in the closed ball $\bar{B}_r(p_0)$, which is compact. Thus, $\{p^*(h_n)\}_{n=1}^{\infty}$ must have a convergent subsequence. If every convergent subsequence of $\{p^*(h_n)\}_{n=1}^{\infty}$ converges to p^* , then (since the sequence is contained in a compact set) $\lim_{n \rightarrow \infty} p^*(h_n) = p^*$ [25], and we obtain a contradiction, so suppose there exists a convergent subsequence $\{p^*(h_{n_m})\}_{m=1}^{\infty}$ with $\lim_{m \rightarrow \infty} p^*(h_{n_m}) = \hat{p} \neq p^*$. Since $\|p^*(h_{n_m}) - p_0\| \leq \|p_{h_{n_m}} - p_0\|$ for all m , taking the limit as $m \rightarrow \infty$ implies that $\|\hat{p} - p_0\| \leq \|p^* - p_0\|$. By Proposition 2, p^* is the unique closest parameter value in ∂R to p_0 under the map $\phi(\cdot, \cdot, \hat{t})$. Therefore, since $\hat{p} \neq p^*$ and is at least as close to p_0 as p^* , we must have $\hat{p} \in R$ under the map $\phi(\cdot, \cdot, \hat{t})$. Thus, $x_0(\hat{p}) \in W^s(x^s(\hat{p}))$, so there exists $\hat{T} > 0$ such that $x_0(\hat{p}) \in \text{int}(\phi(W_{\text{loc}}^s(x^s(\hat{p})), \hat{p}, -\hat{T}))$.

As ϕ and x_0 are C^1 , and by (40), there exist $h' > 0$ and $\delta' > 0$ such that $h \in (0, h')$ and $\|p - \hat{p}\| < \delta'$ implies that $W_{\text{loc}}^s(x_h^s(p))$ under $\hat{T}_d(\cdot, p, h)$ is sufficiently C^1 close to $W_{\text{loc}}^s(x_h^s(\hat{p}))$ under $\phi(\cdot, \hat{p}, \hat{t})$ such that $x_0(p) \in \phi(W_{\text{loc}}^s(x_h^s(p)), p, -\hat{T})$. Thus, for m sufficiently large, $x_0(p^*(h_{n_m})) \in \phi(W_{\text{loc}}^s(x_{h_{n_m}}^s(p^*(h_{n_m}))), p^*(h_{n_m}), -\hat{T})$. Thus, for m sufficiently large, $p^*(h_{n_m}) \in R$ under $T_d(\cdot, \cdot, h_{n_m})$, which contradicts the definition of $p^*(h)$ as the closest point in ∂R to p_0 under $T_d(\cdot, \cdot, h)$. Therefore, we must have that $\lim_{h \rightarrow 0} p^*(h) = p^*$, which proves (12a).

Then, (12b) can be proved by following analogous reasoning as in the proof of Theorem 3, with the following changes:

- All instances of T should be replaced with $T_d(\cdot, \cdot, h)$, including the definitions of $j(p)$ in (9) and $\hat{F}(p)$ in (10).
- All instances of p^* should be replaced with $p^*(h)$.
- For $h > 0$ sufficiently small, there exists $x_h^s(p)$ near $x^s(p)$ stable, and $x_h^u(p)$ near $x^u(p)$ unstable, which are hyperbolic fixed points of $T_d(\cdot, \cdot, h)$ such that $\lim_{n \rightarrow \infty} T_d^n(x_0(p^*(h)), p^*(h), h) = x_h^u(p^*(h))$.
- Since $W^u(x_h^u(p^*(h)))$ is one-dimensional, define \hat{D} and \tilde{D} to be the subsets of $W^u(x_h^u(p^*(h)))$ from \hat{x}_1 to $T_d(\hat{x}_1, p^*(h), h)$, and from \tilde{x}_1 to $T_d(\tilde{x}_1, p^*(h), h)$.

By continuity of $\frac{\partial f}{\partial x}$ and $x_h^u(p)$, and by (12a) and (12b), $\lim_{h \rightarrow 0} \lim_{p \rightarrow p^*(h)} \tilde{F}(p) = \lim_{h \rightarrow 0} \frac{\partial f}{\partial x}(x_h^u(p^*(h))) = \frac{\partial f}{\partial x}(x^u(p^*)) = A(p^*)$, and this proves (12c). (13a) and (13b) can be proved by following analogous reasoning as in the proof of Theorem 2. This completes the proof of Theorem 4. \square

VI. CONCLUSION

This work develops a computationally efficient method with rigorous convergence guarantees for numerically computing the mode of instability for parameterized nonlinear systems

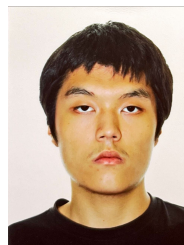
while avoiding the challenge of identifying the CUEP. For parameter values where the system recovers, it averages the Jacobian along the system trajectory from the IC until the final time at which the Jacobian transitions from unstable to stable. It is shown that as boundary parameter values are approached from within the recovery region, this average of the Jacobians converges to the true Jacobian at the CUEP, and it has a unique unstable eigenvalue whose corresponding eigenvector converges to the mode of instability. Under the same conditions, the approximation of the average of the Jacobians obtained from numerical integration, and its eigenvector corresponding to its unique unstable eigenvalue, are shown to converge to the true Jacobian at the CUEP and the mode of instability, respectively, as the step size approaches zero.

The method was first validated on the damped, driven, nonlinear pendulum example subject to a disturbance. By directly finding the CUEP and analytically computing the mode of instability for this low dimensional system, it was shown that the mode of instability could be accurately computed using the proposed algorithm in this case, thereby validating the proposed approach. Then the algorithm was applied to compute the mode of instability for the IEEE 9-bus power system subject to a temporary short circuit. For this higher dimensional power system model, it was no longer straightforward to identify the CUEP and the mode of instability analytically. The method was used to identify the mode of instability in high dimensional parameter space for this system. The identified modes of instability revealed non-intuitive information about the mechanism of instability, and would have been difficult to predict or identify without the use of the proposed method. Future work will include generalizations to other controlling sets, beyond equilibrium points, and developing control design strategies to reduce disturbance vulnerability after identifying the mode of instability.

REFERENCES

- [1] P. Kundur, J. Paserba, V. Ajjarapu, G. Andersson, A. Bose, C. Canizares, N. Hatziairgyriou, D. Hill, A. Stankovic, C. Taylor, T. Van Cutsem, and V. Vittal, "Definition and classification of power system stability ieeecigre joint task force on stability terms and definitions," *IEEE Transactions on Power Systems*, vol. 19, no. 3, pp. 1387–1401, 2004.
- [2] H.-D. Chiang, J. Tong, and K. N. Miu, "Predicting unstable modes in power systems: Theory and computations," *IEEE Transactions on Power Systems*, vol. 8, no. 4, pp. 1429–1437, 1993.
- [3] A. A. Fouad and V. Vittal, *Power System Transient Stability Analysis Using the Transient Energy Function Method*. Englewood Cliffs, NJ, USA: Prentice-Hall, 1992.
- [4] H.-D. Chiang, M. W. Hirsch, and F. F. Wu, "Stability regions of nonlinear autonomous dynamical systems," *IEEE Transactions on Automatic Control*, vol. 33, no. 1, pp. 16–27, 1988.
- [5] A. Michel and V. Vittal, "On the mechanism of transient instability of power systems," *Circuits, Systems and Signal Processing*, vol. 4, no. 3, pp. 413–434, 1985.
- [6] R. Ma, Y. Zhang, M. Zhan, K. Cao, D. Liu, K. Jiang, and S. Cheng, "Dominant transient equations of grid-following and grid-forming converters by controlling-unstable-equilibrium-point-based participation factor analysis," *IEEE Transactions on Power Systems*, vol. 39, no. 3, pp. 4818–4834, 2023.
- [7] A. K. Behera, M. Pai, and P. Sauer, "Analytical approaches to determine critical clearing time in multi-machine power systems," *24th Conference on Decision and Control (CDC)*, pp. 818–823, 1985.
- [8] A. Fouad, V. Vittal, and T. K. Oh, "Critical energy for direct transient stability assessment of a multimachine power system," *IEEE Transactions on Power Apparatus and Systems*, vol. 103, no. 8, pp. 2199–2206, 1984.

- [9] H.-D. Chiang, F. F. Wu, and P. P. Varaiya, "Foundations of the potential energy boundary surface method for power system transient stability analysis," *IEEE Transactions on Circuits and Systems*, vol. 35, no. 6, pp. 712–728, 1988.
- [10] R. T. Treinen, V. Vittal, and W. Kliemann, "An improved technique to determine the controlling unstable equilibrium point in a power system," *IEEE Transactions on Circuits and Systems I: Fundamental Theory and Applications*, vol. 43, no. 4, pp. 313–323, 1996.
- [11] M. W. Fisher and I. A. Hiskens, "Stability of the nonwandering set in the region of attraction boundary under perturbations with application to vulnerability assessment," *SIAM Journal on Applied Dynamical Systems*, vol. 22, no. 4, pp. 3390–3430, 2023.
- [12] M. W. Fisher and I. A. Hiskens, "Hausdorff continuity of region of attraction boundary under parameter variation with application to disturbance recovery," *SIAM Journal on Applied Dynamical Systems*, vol. 21, no. 1, pp. 327–365, 2022.
- [13] M. W. Fisher and I. A. Hiskens, "Numerical computation of critical system recovery parameter values by trajectory sensitivity maximization," *58th Conference on Decision and Control (CDC)*, pp. 8000–8006, 2019.
- [14] M. W. Fisher, "Computing safety margins of parameterized nonlinear systems for vulnerability assessment via trajectory sensitivities," 2025, under review. Preprint available at <https://arxiv.org/abs/2501.07498>.
- [15] M. W. Hirsch, *Differential Topology*, vol. 33 of *Graduate Texts in Mathematics*. Springer-Verlag, 1976.
- [16] C. C. Pugh and C. Robinson, "The c1 closing lemma, including hamiltonians," *Ergodic Theory and Dynamical Systems*, vol. 3, no. 2, pp. 261–313, 1983.
- [17] A. Katok and B. Hasselblatt, *Introduction to the Modern Theory of Dynamical Systems*, vol. 54 of *Encyclopedia of Mathematics and its Applications*. Cambridge University Press, 1999.
- [18] P. W. Sauer and M. A. Pai, *Power System Dynamics and Stability*. 1997.
- [19] P. M. Anderson and A. A. Fouad, *The Elementary Mathematical Model*. Hoboken, NJ, USA: Wiley-IEEE Press, 2003, pp. 13–52.
- [20] *IEEE Std. 421.5-2016, IEEE Recommended Practice for Excitation System Models for Power System Stability Studies*. New York: Institute of Electrical and Electronics Engineers, Inc., 2016.
- [21] J. M. Lee, *Introduction to Smooth Manifolds*. Graduate Texts in Mathematics, Springer, 2 ed., 2013.
- [22] J. Palis, "On morse-smale dynamical systems," *Topology*, vol. 8, no. 4, pp. 385–405, 1969.
- [23] C. Berge, *Topological Spaces (Oliver and Boyd, Edinburgh)*. 1963.
- [24] J. M. Ortega, *Numerical Analysis: A Second Course*. Philadelphia, PA, USA: SIAM, 1990.
- [25] R. G. Sanfelice, "Asymptotic properties of solutions to set dynamical systems," *56th Conference on Decision and Control (CDC)*, pp. 2287–2292, 2014.



stability analysis, control design strategies for improving nonlinear robustness, and power systems.



control, and optimization of complex systems. He was a finalist for the 2017 Conference on Decision and Control (CDC) Best Student Paper Award and a recipient of the 2019 CDC Outstanding Student Paper Award.

Jinghan Wang received Bachelor of Mathematics in Honours Applied Mathematics, with Engineering Specialization in Communication and Control, and Pure Mathematics Minor at the University of Waterloo, Ontario, Canada, in 2023. He is currently pursuing Master of Applied Science with Systems and Control Specialization in the Department of Electrical and Computer Engineering at the University of Waterloo, Ontario, Canada. He works in the dynamics, optimization, and control of complex systems group. His research interests include nonlinear

Michael W. Fisher is an Assistant Professor in the Department of Electrical and Computer Engineering at the University of Waterloo, Canada. He was a postdoctoral researcher with the Automatic Control and Power System Laboratories at ETH Zurich. He received his Ph.D. in Electrical Engineering: Systems at the University of Michigan, Ann Arbor in 2020, and a M.Sc. in Mathematics from the same institution in 2017. He received his B.A. in Mathematics and Physics from Swarthmore College in 2014. His research interests are in dynamics,